Wolfram Jaegermann*, Bernhard Kaiser, Friedhelm Finger, Vladimir Smirnov and Rolf Schäfer

Design Considerations of Efficient Photo-Electrosynthetic Cells and its Realization Using Buried Junction Si Thin Film Multi Absorber Cells

https://doi.org/10.1515/zpch-2019-1584
Received November 13, 2019; accepted January 17, 2020

Abstract: As is obvious from previous work on semiconductor photoelectrochemistry, single junction semiconductors do not provide either the required maximum photovoltage or a high photocurrent for solar water splitting, which is required for efficient stand-alone devices. From these experiences we conclude, that multi-junction devices must be developed for bias-free water splitting. In this article we present our design considerations needed for the development of efficient photo-electro-synthetic cells, which have guided us during the DFG priority program 1613. At first, we discuss the fundamental requirements, which must be fulfilled to lead to effective solar water splitting devices. Buried junction and photoelectrochemical arrangements are compared. It will become clear, that the photovoltaic (PV) and electrochemical (EC) components can be optimized separately, but that maximized conversion efficiencies need photovoltages produced in the photovoltaic part of the device, which are adapted to the electrochemical performance of the electrolyzer components without energetic losses in their coupling across the involved interfaces. Therefore, in part 2 we will present the needs to develop appropriate interface engineering layers for proper chemical and electronic surface passivation. In addition, highly efficient electrocatalysts, either for the hydrogen or oxygen evolution reaction (HER, OER), must be adjusted in their energetic coupling to the semiconductor band edges and to the redox potentials in the electrolyte with minimized losses in the chemical potentials. The third part of our paper describes at first the demands and achievements on developing

***Corresponding author: Wolfram Jaegermann,** Institut für Materialwissenschaften der Technischen Universität Darmstadt, Otto-Berndt-Straße 3, 64287 Darmstadt, Germany, e-mail: jaegermann@surface.tu-darmstadt.de
Bernhard Kaiser: Institut für Materialwissenschaften der Technischen Universität Darmstadt, Otto-Berndt-Straße 3, 64287 Darmstadt, Germany
Friedhelm Finger and Vladimir Smirnov: IEK-5 Photovoltaik, Forschungszentrum Jülich, D-52425 Jülich, Germany
Rolf Schäfer: Eduard-Zintl-Institut für Anorganische und Physikalische Chemie der Technischen Universität Darmstadt, Alarich-Weiss-Straße 8, 64287 Darmstadt, Germany

multijunction thin-film silicon solar cells. With different arrangements of silicon stacks a wide range of photovoltages and photocurrents can be provided. These solar cells are applied as photocathodes in integrated directly coupled PV-EC devices. For this purpose thin Pt and Ni catalyst layers are used on top of the solar cells for the HER and a wire connected RuO_2 counter electrode is used for the OER. Electrochemical stability has been successfully tested for up to 10,000 s in 0.1 M KOH. Furthermore, we will illustrate our experimental results on interface engineering strategies using TiO_2 as buffer layer and Pt nanostructures as HER catalyst. Based on the obtained results the observed improvements, but also the still given limitations, can be related to clearly identified non-idealities in surface engineering either related to recombination losses at the semiconductor surface reducing photocurrents or due to not properly-aligned energy states leading to potential losses across the interfaces.

Keywords: artificial leaf; interface engineering; multi-junction solar cells; photoelectrochemistry; platinum nanoparticles electrocatalyst; thin-film silicon.

1 Introduction

The energy demands of mankind cannot be delivered by C-based fossil fuels in the near future due to the limitations of given resources, even more if the expected growth in energy utilization of the developing countries is taken into account [1–3]. Additionally, the related emission of CO_2 and other greenhouse gases will most probably lead to a heating of the atmosphere with severe climate changes on earth. Despite the fact that fossil fuels are remains of solar photosynthesis running over millions of years the yearly yield of fuel generation based on biomass is considered to be not efficient enough to substitute the used resources on a short time scale.

As a consequence, renewable and carbon free energy from wind and solar radiation have been considered for a long time to be the most promising alternatives, but were always considered to be too expensive to be used in the near future. This has been changed with drastic improvements of technology, which have led to competitive electricity costs. In addition, the available yearly resources are more than sufficient to fully replace fossil fuels and furthermore are able to cover the increasing energy demand in the future. However, as wind and solar radiation are volatile sources efficient energy storage and transport means are needed to store the produced electric energy, which so far cannot be realized with e.g. batteries or other appropriate and efficient storage systems [1, 2, 4, 5]. Mimicking nature for producing a “solar fuel” seems to be very promising: In photosynthesis the sun’s energy is converted to form chemical compounds with a high energy

content, i.e. carbohydrates, from compounds with low energy content, i.e. water and CO_2. For artificial photosynthesis the simplest chemical compound with a high gravimetric energy density is hydrogen. Hydrogen is an extremely versatile fuel, since it can either be burned directly in a combustion engine or it can be used to produce electricity in a fuel cell [6]. Furthermore, it can be converted to liquid and gaseous fuels with a higher energy density, i.e. formic acid, methanol and methane, by the Fischer-Tropsch or Sabatier processes [7–11]. Using hydrogen is a clean technology, since the educts are at the same time the products, i.e. water, forming a closed-loop reaction cycle.

Hydrogen is the most abundant element in the universe. On earth it exists only in bound form mainly to oxygen as water. Therefore, the production of clean hydrogen using renewable energy sources in an economically feasible way is a major challenge. The synthesis of hydrogen by electrolysis with electric power from photovoltaics is feasible, but the combination of these techniques is rather expensive if compared to the standard processes, which are used nowadays, employing natural gas or oil [12]. Still, there exist already a few pilot projects in Germany using hydrogen as energy carrier generated by surplus wind and solar energy [13, 14]. Artificial photosynthesis using semiconductor/electrolyte contacts to split water is considered to be the "holy grail" of photoelectrochemistry since the discovery of light induced H_2 formation from H_2O as presented by Fujishima and Honda in 1972 [15]. They used an n-TiO_2 photoanode irradiated with ultraviolet (UV) light to electrolyze water in a light driven process forming hydrogen and oxygen. However, TiO_2 and very many wide band gap oxides have large bandgaps above 3 eV and only light in the ultraviolet region will be absorbed. As the related UV light is only a minor part of the solar spectrum the obtained conversion efficiencies are rather low typically in the range of about 0.1%. Identifying the right semiconductor materials with appropriate bandgaps and adjusted charge transfer properties allowing HER as well as OER without any additional electrical and chemical bias remains critical for the realization of efficient devices. They have been called artificial inorganic leaves [16] to indicate their relation to the photosynthesis conversion process in leaves which produce fuels from water and sunlight.

Since 1972 intensive research on photoelectrochemical H_2O splitting devices has started and very many more semiconductor electrodes to be used for water splitting have been investigated, in most cases with limited success (see for example [17, 18]). Only rather few systems have provided reasonable conversion efficiencies but very often with different shortcomings in their design which provide additional support. Therefore, these studies mainly serve as a proof of principle: Heller and Vadimsky reported already in 1981 an efficiency of 12% for hydrogen production from p-InP photocathodes covered with small platinum metal islands.

But they did not reach sufficient stability of their photoelectrode in contact to the electrolyte and even worse it did not deliver enough voltage on its own to drive the water splitting reaction: to reach the voltage for driving H_2O electrolysis an external bias voltage had to be added to the photovoltage provided by the photocathode [19]. Recently, InP based electrodes have been further developed by Lewerenz et al. [20]. The first device capable of generating the photovoltage, which is required for the water splitting reaction, was presented by Khaselev and Turner in 1998 [21]. They used a tandem-structure of p-GaInP as photocathode supported by a GaAs solar cell to generate the necessary total photovoltage and reached an overall solar-to-H_2 (STH) efficiency of 12.4%, but the device suffers from stability problems and high production costs. Nevertheless, this study can be considered as an important step forward as it showed the need of employing a tandem cell arrangement to overcome the single small band gap semiconductor limitation on photovoltage. Only the combination of several semiconductor absorber materials allows to achieve higher theoretical photovoltaic conversion efficiencies and 3–5 based multijunction solar cells provide the highest practical conversion efficiencies [22–24]. In addition, with the right combination of materials higher photovoltages can be reached. Another tandem cell device based on AlGaAs and Si was presented by Licht and coworkers in 2000 [25]. An efficiency of 18.3% was reported at a maximum power photopotential of 1.3 V. It should be noted, that the authors did not immerse the PV cell into the electrolyte, that the performance was determined at AM 0 and that the area of the electrodes was a factor of 45 larger than the actual area of the absorber itself. In 2011 a triple cell based on thin film silicon was presented by Reece et al. reaching a total efficiency for hydrogen production between 2.5% and 4.7% [26]. But even for this case the estimated costs per kg hydrogen were still too high despite using cheap thin film solar cells, and the long-term stability was not sufficient.

The general applicability of photoelectrochemical water splitting was proven with these examples, but in many cases the devices do not deliver the required voltage for bias free water splitting. Furthermore, reported efficiencies have to be carefully assessed on how they have been determined. In recent contributions the proper use of terminology and determination of conversion efficiencies have been defined [27, 28]. A large number of review articles and books have been published about photoelectrochemical systems in recent years, some recent reviews are found in [17, 18, 29] and references given therein.

The fundamental part of this review has already been published previously, but with some other intention in mind [30]. To omit these parts would lead to a drastically reduced clarity in this manuscript about buried-junction PEC-devices. Therefore, we kept the reformulated fundamental block completely, and we added the overview on our recently obtained results on Si-based multi-junction

structures for PEC water splitting in the second part. With that we want to emphasize our ideas on the relevant engineering strategy, which must be followed to realize an efficient and competitive photo-electro-synthetic cell. These conceptual ideas were the guiding lines which have been followed in our research and development strategy within the framework of the DFG priority program (see Figure 1). The electric coupling of solar cells to an electrolyzer cell provides the reference point and must be considered as the benchmark for any solar light to H_2 converting device. Similar efficiencies must also be realized with artificial leaf approaches. For this reason, we have addressed device structures where the photovoltaic component of the cell is inherently integrated to the electrolyzer part of similar size and form. At least one electrode is in contact with the electrolyte and thus will form a compact cell compartment (hydrogen generator array or pixel). Larger H_2 forming solar energy conversion modules may finally be put together from such converter pixels (as in Si solar modules) or may even be manufactured as larger modules by using thin film deposition and structuring technologies (as compared to thin film solar cells, see for example [31]). In Figure 1 a standard photoelectrochemical cell arrangement is shown which was further developed to a photo-electro-synthetic cell pixel (see also the contribution of Finger et al. in this special edition of ZPC). Some of the the integrative concepts have been used and proven to provide promising development routes in the meantime, as will be discussed in some more detail later on. However, a final and competitive

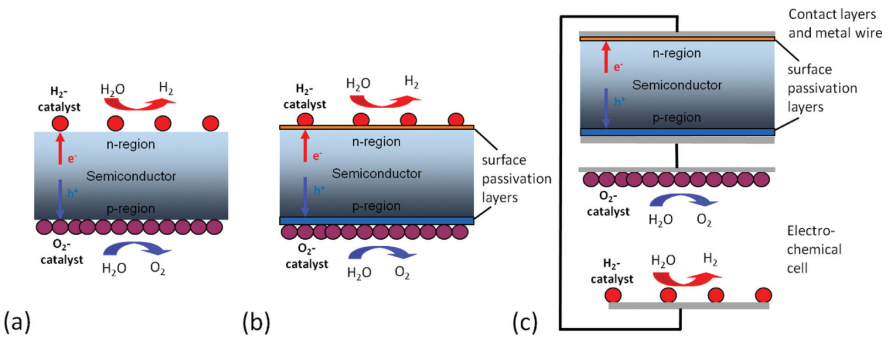

Fig. 1: Schematic representation of different semiconductor based "artificial leaf" structures providing the same active area of the PV and EL component (PEC-pixel): (a) direct semiconductor/electrolyte junctions including co-catalysts for the HER and OER reactions, (b) buried junction photovoltaic cells coupled to co-catalysts used as photoelectrochemical cells, (c) solar cell connected to an electrochemical cell with the HER and OER half cell reactions. The absorbing semiconductor PV device is in all cases approximated by a thin film based p-i-n structure. Reprinted by permission from Springer Nature: Springer, *Photoelectrochemical Solar Fuel Production*, S. Gimenez, J. Bisquert (Eds.) ©(2016).

solution is still not available and will also be discussed in more detail in the course of this contribution. Therefore, further research efforts are needed which will be presented in an outlook at the end of this paper.

2 Fundamental considerations of semiconductor-based water splitting

2.1 Buried photovoltaic vs. photoelectrochemical devices

Efficient artificial photosynthesis with promising conversion efficiencies and with technologically competitive costs can only be realized, if the photovoltaic part is efficiently coupled to the electrolyzer function. This can be realized by the connection of a solar cell to an external electrolyzer via cables as shown in Figure 1c, or one may hope that semiconducting absorber layers in contact to the electrolyte may as well form the energy converting junction and also act as electrocatalysts. This can usually not be expected and therefore co-catalyst deposits are used as shown in Figure 1a. For competitive efficiencies all systems need to show the same performance levels. This will be possible, if a number of succeeding elementary processes are coupled to each other with minimized losses, which basically are the same for all light to fuel converter systems: 1. broad band light absorption covering the spectral distribution of sunlight, 2. optimized charge carrier generation with a maximized splitting of the chemical potential of the minority carriers (electron and holes) avoiding internal charge recombination, 3. vectorial separation of the minority carriers across the involved interfaces forming the contacts, as well as 4. the efficient electrocatalytic production of H_2 and O_2 from H_2O in separated compartments (hydrogen evolution reaction HER, oxygen evolution reaction OER). For a fair comparison of performance in integrated device structures the absorber layer defines the lateral dimensions of the device (photoelectrochemical arrays or pixels), excluding connections of large-scale PV converter arrays with external electrolyzer cells (here the application and balance of systems costs are considerably different). But, for any technological competitive device a combination of complimentary components, which allow to combine efficient and stable photovoltaic converter arrangements with efficient catalysts, are needed preferentially based on low cost, abundant, and non-hazardous materials. There are a lot of different research strategies discussed in literature and summarized and defined in a paper by Nielander et al. [28]. If one is willing to follow his definitions may be a matter of taste in some cases, but at least it gives a nice survey of

what can be done. From our consideration of an adequate terminology a “photo-electro-chemical cell" (PEC) may not be restricted to devices where the semiconductor/electrolyte contact defines the energy converting space charge layer, which is equivalent to the diffusion voltage for solid state contacts, but that also interface engineered buried junction cells containing a semiconductor/interface layer/catalyst/electrolyte junction should be considered as buried junction PEC cells. Indeed, numerous water splitting PEC cells studied in literature contain surface modification layers and metallic co-catalysts (sometimes formed within the electrolyte) and therefore the distinction is somewhat arbitrary (for a recent survey of investigated junctions see [18]).

As we are convinced, that the above given primary steps of the photoelectrochemical conversion need to be realized with minimized losses we will concentrate in our discussion on buried junction photoelectrochemical cells as shown in Figure 1b, which provide, to our understanding, the most realistic artificial photosynthetic system in the foreseeable future. A more detailed discussion of this approach can be also be found here [30]. A further limiting factor that should not be neglected is the small diffusion coefficient of protons generated at the anode side together with oxygen which have to migrate from the anode to the cathode side in the electrolyte.

Promising device structures can only be realized in the short term, and maybe also in the long term, by the combination of efficient solar converters as provided by and equivalent to solar multijunction cells with highly active electrolyzer components for HER and OER. For their realization knowledge-based engineering strategies are needed, which will allow to couple the PV absorber component to the electrocatalysts with minimized losses in photovoltage and photocurrent. We will present in the following our understanding of the decisive mechanisms involved, which are discussed based on experiments on well-defined semiconductor junctions as model and reference systems. Further advanced design approaches may apply the identified design strategies to employ more promising materials and material combinations as well as adopted device structures.

If we compare the different PEC junctions using either a direct semiconductor/electrolyte contact, photo-electrochemical junctions using buried solid-state contacts immersed to the electrolyte, and photovoltaic cells connected to an electrolyzer with each other (Figure 1), it seems evident, that they are rather equivalent to each other. The above discussed inherently connected elementary processes are equivalent to each other and any energy (voltage) or current loss (recombination) must be avoided. Or one may turn this argument around, if the junction properties and related charge carrier dynamics show strong loss processes in either photovoltage or photocurrent one may not expect high efficiencies; this is true and comparable for all of the different conversion structures discussed. Therefore, most

strategic concepts are transferable from one device to the other and the different systems must be optimized in an equivalent way. Because of our background in thin film photovoltaic research, we will start our discussion of the involved processes from thin film solar cells and transfer the deduced concepts and boundary conditions to thin film based buried junction photo-electrochemical cells. An efficient photo-electrochemical cell in which the semiconductor/electrolyte contact provides the photovoltaic function as well as the catalytic function can hardly be expected to provide efficient devices. Already the addition of a co-catalyst layer leads to buried junctions. The performance conditions of efficient devices, as will be exemplified in more detail later on, are: 1. The operational photovoltage of the water splitting device structure must be in the range of 1.5–1.9 V depending on the involved (over)voltage losses in the electrochemical cell. This translates to the photovoltage which is comparable to the maximum power point photovoltage of a solar cell. 2. The photocurrent quantum efficiency must approach 1 for all photons absorbed by the absorber layers above their band gap (neglecting any parasitic absorption and reflection losses). Thus, one may already conclude here that absorber layers and junctions which are not able to perform well in PV devices will also not perform well in PEC devices.

Based on our experience and the results published in literature we expect that most likely only buried junction photo-electrochemical cells based on multiabsorber PV structures will provide the most probable (may be the only reasonable) route to an economically competitive "artificial leaf" for solar fuel production (compare Figure 1). However, the concepts and boundary conditions derived for these structures are also mostly valid for single crystalline or nano structured devices. The challenges and research needs are very similar to each other as we will stress in our contribution.

As first step multispectral broadband light absorption and efficient generation and separation of light induced electron-hole pairs must be considered. Here, established semiconductors are preferentially used as they provide best results for broadband charge carrier generation. For highly efficient semiconductors in solar cell applications the electron-hole pair generation approximates a quantum efficiency of one ranging in principle from its fundamental bandgap to the UV cut-off of the solar spectrum (neglecting at first parasitic losses due to additional sequences of contact and catalyst layers). If multiabsorber structures are applied the spectral absorption range is defined by the bandgap difference and absorption coefficients of the combined absorber materials [23, 32]. The non-equilibrium electron n* and hole h* concentration inside the PV converter is given by the product of generation rate G and minority carrier lifetime τ, which leads to the difference in the chemical potential of electrons and holes $\Delta\mu_{e-h}^{*} = kT \ln n^{*}/p^{*}$,

equivalent to the splitting of quasi Fermi levels of electrons and holes, respectively, $nE_F^\star - pE_F^\star$ under illumination. This difference in quasi Fermi levels or chemical potentials of electrons and holes of the minority carrier provides the driving force for any electrochemical charge transfer reactions and are the maximum photovoltage the PV converter can deliver [32]. As boundary condition for photoelectrochemical water splitting, the photovoltaic converter system must be able to provide a minimal difference in the chemical potentials of minority carriers (electrons and holes) $\Delta\mu_{e-h}^\star$ for non-equilibrium conditions under illumination. This value is equivalent to the usable (operative) photovoltage ${U_{ph}}^{op}$ of the PV-converter which must exceed a minimum value of about 1.6 V for water splitting as will be discussed in more detail below. This value corresponds to an open circuit photovoltage of about ${U_{ph}}^{oc}$ of 1.7–1.9 V for PV converters of good performance. As additional condition for high conversion efficiencies the quantum efficiencies of the reacting minority carriers should approach 1, which means that every absorbed photon should produce one light induced electron-hole pair. The contacts and co-catalysts must be adjusted to allow for their efficient separation from each other leading to a maximized operational photocurrent ${j_{ph}}^{op}$ (the physical materials properties needed to reach this boundary condition will also be exemplified below).

For idealized electric power producing solar cells the efficiency of the converter is given by (see e.g. [32]):

$$\eta_{el} = U_{ph}^{oc} \cdot j_{ph}^{oc} \cdot FF/P_{hv} = U_{mpp} \cdot j_{mpp}/P_{hv}, \tag{1}$$

with ${U_{ph}}^{oc}$ times ${j_{ph}}^{sc}$ as the open circuit photovoltage times the short circuit photocurrent times the FF as fill factor, which translates to the electric power at the optimum operational (maximum power) point of the solar cell of U_{mpp} times j_{mpp} (P_{hv} is the light power incident onto the solar cell). The current-voltage curve is given by eq. 2:

$$j(U) = j_0 \cdot \left[\exp\left(\frac{eU}{kT}\right) - 1\right] - j_{ph}, \tag{2}$$

with j as classical notation for the current density. It is evident, that at the maximum values of either U_{ph} and j_{ph}, respectively, in the current voltage curve of the solar cell the conversion efficiency of the converter is 0 (at ${U_{ph}}^{oc}$ $j_{ph} = 0$ or at ${j_{ph}}^{sc}$ $U_{ph} = 0$). For real solar cells eq. 2 has to be modified to account for loss processes due to charge carrier recombination R_p and electric resistances in charge carrier transport or charge transfer R_s (eq. 3):

$$j(U) = j_0\left[\exp\frac{U - jR_s}{kT} - 1\right] + \frac{U - jR_s}{R_p} - j_{ph}. \tag{3}$$

For ideal solar cells R_s has to approach 0 and R_p has to approach infinity. If we now add the additional functionality of the electrochemical HER and OER reactions in photoelectrochemical devices, the boundary conditions as defined by the solar converter still hold. However, it cannot be expected that eq. 2 will be valid. A modified version of eq. 3 must be applied accounting for the additional electron and hole transport, transfer and reaction steps, involved. For the mathematical description of electrocatalytic devices working in the dark usually the Butler-Volmer equation is applied [33], which is given by eq. 4:

$$j = j_0 \left[\exp\left(\frac{(1-\alpha)e\eta}{kT} \right) - \exp\left(\frac{-\alpha e\eta}{kT} \right) \right]. \tag{4}$$

It is used for any redox reaction involved (HER: $\varepsilon°(H^+/H_2)$ and OER: $\varepsilon°(H_2O/O_2)$ depending on the deviation from the equilibrium potential $\eta = \varepsilon(j) - \varepsilon°(j = 0)$. The catalytic efficiency is given by the exchange current density j_0 at equilibrium conditions $\varepsilon°(j = 0)$. To catalyze the H_2O redox reactions after charge separation in the solar converter component (nano-sized) noble metals, earth abundant transition metal compounds as solids or molecular (biomimetic) coordination compounds are generally applied as electrocatalysts. The aim is to reach maximized currents for lowest values of overvoltage, as the photovoltage of the converter must be used to drive the HER and OER of the water splitting device structure. For a rather ideal PEC system the overall current-voltage behavior is then given by the sum of all current-voltage dependencies within the circuit as given in eq. 5 [34]:

$$\underbrace{V_{PV-EC(j)}}_{\substack{j-V \\ \text{PECdevice}}} = \underbrace{V_{PV(j)}}_{\substack{j-V \\ \text{Solarcell}}} - \Delta E_{H_2O} - \underbrace{\eta_{OER}(-j)}_{\substack{j-V \\ \text{Anode}}} + \underbrace{\eta_{HER}(j)}_{\substack{j-V \\ \text{Cathode}}} + \underbrace{jR}_{\substack{\text{Ohmic} \\ \text{loss}}} \tag{5}$$

For such ideal systems there are no time transients visible for chopped illumination as all electron-hole carrier dynamics are considerably faster than typical chopping frequencies. Whenever in current voltage curves transients are evident slow charge carrier reactions must be taken into account, which usually are due to trapping/detrapping reactions of electrons/holes [36]. In such cases the ideal and simplified current voltage behavior shown in Figure 2 does not hold any more and more complicated numerical models have to be taken into account (see e.g. [37]). In these cases, however, the performance values of the PEC device are drastically reduced.

As we will discuss in more detail later on there may be additional losses, which may be added to the sum of loss mechanism, which are due to potential losses at phase boundaries (interfaces) between the PV absorber and the catalyst

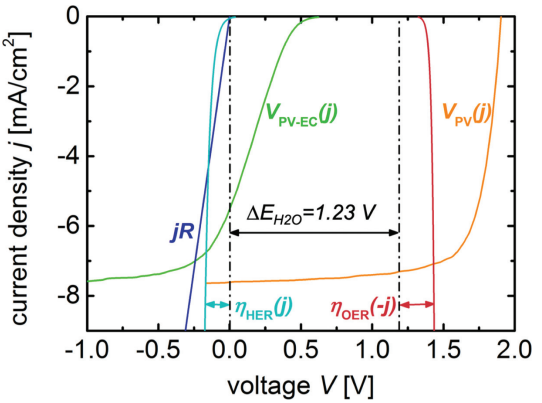

Fig. 2: Current density voltage curves of a rather ideal integrated PEC cell as shown in Figure 1. The overall current voltage curve is an in-series connection of solar cell, anodic OER and cathodic HER, and ohmic loss. The *j-U* dependencies are calculated from eqs. (2) to (5). The performance is given from these two electrode measurements at the value of 0.0 V as the value of $\Delta E_{H_2O} = 1.23$ V has been subtracted (adapted from [35]).

layer $\Delta\Phi_{interf}(j)$. They are due to double layer potential drops induced by trapped charge carriers.

2.2 Boundary conditions for obtaining the required photovoltages

As discussed above the photovoltaic converter either as solar cell connected to the electrolyser or as component of the photoelectrochemical cell must provide the necessary photovoltage (chemical potential difference of electrons and holes under illumination) as driving force for the HER and OER reaction as well as any additional voltage losses e.g. due to Ohmic losses because of proton transport. In using the terminus of solid state physics the difference of the quasi Fermi levels of electrons and holes $\Delta\mu^{\star}_{e-h} = {}_nE_F{}^{\star} - {}_pE_F{}^{\star}$ generated inside the solid semiconductor device, which is the maximum photovoltage which may ideally be outcoupled from the PV converter, must exceed the difference of the half cell potentials of the HER and OER as well as all additional kinetic losses across given interfaces.

$$\Delta\mu^{\star}_{e-h} = {}_{\mathrm{n}}E^{\star}_{\mathrm{F}} - {}_{\mathrm{p}}E^{\star}_{\mathrm{F}} \geq \mathrm{e}\cdot U_{\mathrm{ph}} > -e\cdot\left(\varepsilon^{\circ}(H_2/H_2O) - \varepsilon^{\circ}(O_2/H_2O)\right) = 1.23\ \mathrm{V} \quad (6)$$

Thus, the value of U_{ph} needed for light induced water splitting without adding an additional external bias must exceed the difference of the electrochemical potentials of the reductive and oxidative water splitting reactions $\Delta E_{\mathrm{H_2O}}$ by the

amount of a sum of kinetic losses as reaction overpotentials which are dependent on the exchange current densities and further resistive losses in the circuit given by $j_{ph} \times R$ and interface double layer losses given by $\Delta\Phi_{interf}(j)$ for each involved interface. An estimate of the current density provided by the PV converter, which is directly proportional to the solar to H_2 conversion efficiency (see eq. 12) will define the needed overvoltages and ohmic losses and thus a minimum operational photovoltage ${U_{ph}}^{op}$, which must be provided by the PV-converter in the working photoelectrochemical device. This minimum ${U_{ph}}^{op}$ does not exist for photovoltaic converters producing only electric power (see eq. 1), a reduction in photovoltage may be compensated by an increased photocurrent and vice versa. As it is immediately clear, most of the prominent single absorber PV cells, which have reached high solar to power efficiencies, have fundamental bandgaps below 1.5 eV and do not provide high enough open circuit photovoltages ${U_{ph}}^{oc}$ needed for H_2O splitting. As a consequence, multiple PV components must be added in series for efficient H_2O splitting. Here different arrangements have been suggested [18, 28]. We show only two examples: An integrated tandem cell as photocathode as used in our experiments and a combination of two separated photo electrodes (photocathode plus photoanode) as to be used for non-integrated PV converters; the latter arrangement is preferentially to be used in part for the investigation of single photoelectrodes even when they do not provide sufficient photovoltage for H_2O splitting.

The kinetic overpotential losses depend on the kinetic demands for high electron exchange rates. Both half-cell reactions involved in water splitting, the HER and OER, are multi electron transfer reactions in which two or four electrons must be exchanged across the interface. Overall the PV converter must deliver four electrons and holes step by step to form two molecules of H_2 and one molecule of O_2:

$$4H^+ + 4e^- \rightarrow 2H_2 \qquad \varepsilon^\circ(H^+/H_2) = 0\ \text{V} \tag{7}$$

$$4H^+ + 4e^- + O_2 \rightarrow 2H_2O \qquad \varepsilon^\circ(H_2O/O_2) = 1.23\ \text{V} \tag{8}$$

$$2H_2O \xrightarrow{h\nu} 2H_2 + O_2 \quad \Delta E_{H_2O} = \varepsilon^\circ(H^+/H_2) - \varepsilon^\circ(H_2O/O_2) = -1.23\ \text{V} \tag{9}$$

In the literature there is an extensive discussion on the energetic position of the conduction band minimum and valence band maximum with respect to the HER and OER redox potentials, in short the band edges must straddle the redox potentials. If this is the case depends also on the influence of interfacial double layer potential drops, which are known to be different for different surface orientations [38, 39]. However, these often-applied considerations may be non-valid if buried junctions or trap assisted kinetic shifts of band edge positions are considered. Any band alignment depends strongly on the solid/electrolyte

interfacial structure and chemical composition under operation (illumination) conditions and cannot be deduced in a reliable way from experiments in the dark. At first, the HER and OER redox potentials shift in their values depending on the pH of the solution; e.g. from their values at pH = 0 (1 N [H^+]) by 59 mV/pH. This shift is well known and usually considered for band edge alignment to the OER or HER half-cell redox potentials. However, the band edge positions of the semiconductor may also shift by 59 mV/pH for an oxidic surface. To what extent oxidic surfaces are formed during exposure to the electrolyte or with the involved reactions are often not properly studied; a reduced or no shift of band edges is expected for less ionic or more covalent semiconductors. But, in addition, the band edges tend to shift also due to the trapping of charge carriers in existing or formed surface states during illumination [40–44]. The same is true if a semiconductor/metal (electrocatalyst)/electrolyte junction is forming the contact. These facts may lead to a modified rearrangement of band edge positions under operation conditions with illumination compared to the values given in the dark.

As already introduced above the PV converter of the PEC cell must provide the required photovoltage, which is needed to drive the water splitting reaction. Considering all kinetic losses this translates to the equation:

$$U_{\mathrm{ph}}^{\mathrm{op}} > \Delta E^{\mathrm{op}} = \Delta E_{\mathrm{H_2O}} + \eta_c + \eta_a + j_{\mathrm{ph}} \cdot R + \sum \Delta\Phi_{\mathrm{interf}}(j) + \Delta U_{cs}(j) \qquad (10)$$

This photovoltage must at least be equal or exceed the electrochemical potential difference ΔE^{op}, which would be needed for driving the water splitting reaction in a dark electrolysis mode, with the addition of some correction terms deduced from the coupling of the PV converter. In numbers we have to consider the thermodynamic electrochemical potential difference related to water splitting $\Delta E_{\mathrm{H_2O}}$ given by 1.23 V. Additionally, potential losses for driving noticeable photocurrents from the interior of the PV component to the surfaces have to be considered, which are given in a first approximation by the gradients of the electrochemical potentials of electrons and holes grad ${}_{\mathrm{n}}E_{\mathrm{F}}{}^{\star}$ and grad ${}_{\mathrm{p}}E_{\mathrm{F}}{}^{\star}$ to drive the charge carrier separation ΔU_{cs} (j); the values needed for electron and hole extraction depend on the concentration distribution and mobilities of the respective charge carriers and the remaining voltage drop in the PV converter and are given by:

$$\Delta U_{\mathrm{cs}} \approx U_{\mathrm{ph}}^{\mathrm{oc}} - U_{\mathrm{ph}}^{\mathrm{mpp}}, \qquad (11)$$

with $U_{\mathrm{ph}}^{\mathrm{mpp}}$ being the photovoltage at the maximum power point. The sum of the current depending double layer potential drops $\sum \Delta\Phi_{\mathrm{interf}}(j)$ is due to non-ideal semiconductor junction behavior e.g. Fermi level pinning (see below and [30]). For the given estimation we assume this value to be zero. To be added are the

overvoltages η_c and η_a for the HER and OER, respectively, needed for the provided photocurrent densities (approximated as 0.05 and 0.3 V, respectively, assuming highly efficient electrocatalysts and typical PV current densities of 20 mA/cm^2). The Ohmic losses in the circuit $j_{ph} \times R$ e.g. given by the resistance of the electrolyte solution between cathode and anode to carry the photocurrent j_{ph} must be made as small as possible assuming for our estimate a value of only $<$0.05 V. This small value may be possible for the device arrangement shown in Figure 1c; in cases where e.g. the H^+ transport has to pass from the front to the backside of the cell or for neutral solutions this value may be considerably larger [37]. Assuming ideal interface properties without any additional potential loss $\Delta\Phi_{interf}(j)$, the photovoltaic converter must provide an operational photovoltage $U_{ph}{}^{op}$ of at least 1.6 V assuming optimistic values for the different kinetic loss values on the right-hand side of equation (10) (1.23 + 0.05 + 0.3 + 0.05 V). The energetic conditions are schematically shown in Figure 3 for a one band gap absorber system, which in principal is equivalent for tandem or multi-junction structures (neglecting the gradients of the quasi Fermi levels, serial resistive losses, and interface potential losses).

One factor, which is often forgotten, in such estimates of needed photovoltages is the fact that the PV device/component must be operated close

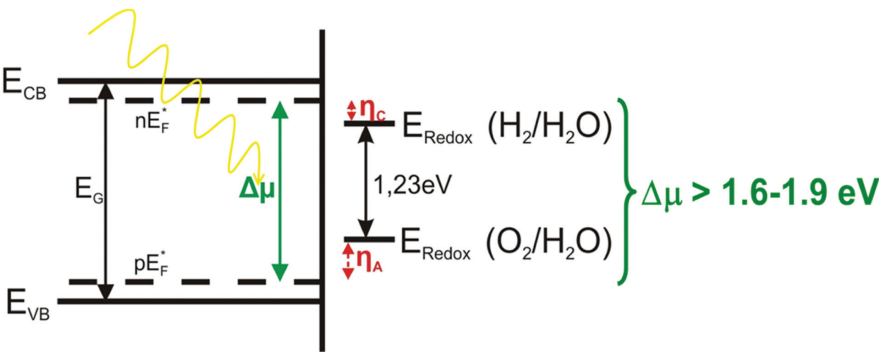

Fig. 3: Schematic energy diagram for a single absorber PV converter coupled to electrochemical water splitting reactions under illumination assuming an ideal band edge arrangement. In most real cases as in PEC devices the electron and hole contact would be situated at opposite parts of the absorber. At photocatalytic particles also the given arrangement may be possible. A minimum $\Delta\mu$ value of 1.6 eV may be calculated for the open circuit photovoltage assuming ideal conditions ; depending on the quality of the PV absorber material for the operational photovoltage an additional ΔU_{cs} of 0.3 eV is needed for achieving reasonable photocurrents (kinetic driving force for efficient charge separation within the PV component) as approximately given for MPP conditions. Reprinted by permission from Springer Nature: Springer, *Photoelectrochemical Solar Fuel Production*, S. Gimenez, J. Bisquert (Eds.) ©(2016).

to the maximum power point to reach high operational photocurrents, which will add an additional voltage difference $\Delta U_{cs} = U_{ph}^{oc} - U_{ph}^{mpp}$ of about 0.3 V to the operational photovoltage $U_{ph}{}^{op}$ even for good photovoltaic absorbers. Depending on electron and hole transport properties inside the semiconductor bulk and the surface conditioning (effecting surface recombination) the quality of the photovoltaic converter will also be expressed in a small value between the open circuit potential and the potential of the maximum power point which is equivalent to the operational voltage of the solar cell giving the highest conversion efficiencies (see. Eqs. 11 and 12). For bad semiconductor materials, which will only lead to poor photovoltaic converters with low fill factor, the photocurrent will only slowly rise with voltage, which translates to a much larger difference of the MPP photovoltage compared to the open circuit photovoltage.

The performance of a water splitting device is determined by the photocurrent flowing at the operational photovoltage. This voltage must be large enough to drive the H_2O splitting reaction including all kinetic losses (overpotentials, interface losses, and ohmic losses) in a two-electrode arrangement without using additional electric (for example with potentiostats) or chemical bias (using concentration differences). Thus, comparing the performance data of a PV electric power producing solar converter vs. a H_2O splitting photoelectrochemical device, it follows that the solar to H_2 conversion effciency η_{STH} as given by eq. (12) is only determined by the photocurrent j_{ph} achieved in the two electrode arrangement. Whether the PV converter provides a sufficient operational photvoltage to run the water splitting reaction can be estimated as discussed above. If reasonable values of the overvoltages with the given electrocatalysts are available, the photovoltage of the PV converter at the MPP in relation to the thermodynamic H_2O splitting potential multiplied with the achieved photocurrent provides a realistic upper value for an estimate of the H_2 (STH) conversion efficiency (assuring a faradaic efficiency of 1):

$$\eta_{STH} = \Delta E_{H_2O} \cdot j_{ph}/P_{h\nu} < U_{ph}^{op} \cdot j_{ph}/P_{h\nu} \quad \text{with } U_{ph}^{op} > \Delta E_{H_2O} = 1.23 \text{ V} \qquad (12)$$

If we compare the open circuit photovoltages reached for high efficiency solar cells it becomes immediately clear that most of the single absorber cells do not reach a sufficiently high photovoltage to drive the water splitting reactions without any bias [30]. For the best photovoltaic devices there is an evident dependence of the photovoltage vs. bandgap given by $U_{ph}{}^{oc} = 1/e * (E_G - 0.4 \text{ eV})$ [23, 32]; for most PV converters of thin film semiconductors it is hard to reach values for $U_{ph}{}^{oc}$ beyond $1/e * E_G/2$ [45]. As a consequence, high conversion efficiencies are not expected for single absorber cells, but multijunction cells are needed (remember that for estimating the operational photovoltage $U_{ph}{}^{MPP}$ must be considered). As

an estimate of the possibly achievable STH efficiencies in dependence of absorber bandgap(s) a number of studies have been recently published [46–48] following the original approach of Bolton [49]. Depending on the used parameters of photoelectrochemical water splitting devices different bandgaps and achievable performance data may be calculated: Based on a needed U_{ph}^{op} of 1.6 V, which translates to a U_{ph}^{oc} of 1.9 V a single absorber layer will provide at best a theoretical PV power efficiency of about 15%, which translates to a maximum STH efficiency of about 12%. In case of a tandem cell a minimum bandgap combination of 1.1 and 1.7 eV may be needed ($U_{ph}^{oc} = 0.7 + 1.3$ V assuming $U_{ph}^{oc} = 1/e * (E_G - 0.4$ eV), which may provide STH efficiencies of about below 30%. For less ideal absorber materials ($U_{ph}^{oc} \leq 1/e * E_G/2$) the expected efficiencies must be corrected to considerably lower values.

A valid STH conversion efficiency can only be determined in a two-electrode arrangement without potentiostatic correction of resistive losses in the circuit. However, for many electrodes under investigation only part of the operative voltage may be reached especially when photoactive half cells (photocathodes or photoanodes) are investigated. In this case, part of the operative photovoltage may be provided by an external bias U_{bias}. The light induced efficiency is then equivalent to the electric energy provided by the illumination of the photoactive component in H_2 production given by the photovoltaic power stored j_{ph} (ΔE_{H_2O}-U_{bias}). Thus, it converts to an energy saving efficiency η_{STH}^{ass} given by:

$$\eta_{STH}^{ass} = \frac{j_{ph}(\Delta E_{H_2O} - U_{Bias})}{P_{hv}} \tag{13}$$

This electric power may also be provided by an external solar cell coupled to the two half cells with a maximum energy saving efficiency if it runs at the maximum power point. However, some boundary conditions are still valid even if assisted efficiencies are discussed: Two electrode arrangements, no potentiostate and only the HER and OER reactions have to be considered. Any STH conversion efficiency given for a bias outside the value of $\Delta E_{H_2O} = 1.23$ V (more negative than the reversible hydrogen potential or more positive than the reversible oxygen potential) are not valid. The discussion of STH efficiencies are also not reasonable if sacrificial donors or acceptors are used.

These estimates indicate that the PV converter component and the electrolyzer functionality as given by the electrocatalysts and the ohmic losses as given by the device arrangement must be adjusted to each other. For a test whether the PV component in a photoelectrochemical cell will provide the perfomance data needed for water splitting either electric power producing solar cells with solid state contacts or alternatively photoelectrochemical cells with electrolyte

contacts containing a reversible and fast redox couple of appropriate redox potential can be measured. These tests will provide a measure of the PV performance of the included semiconductor device independent on the more demanding electrolyser function and possibly needed interface passivation layers. If the PV component in these reference measurements does not provide the needed converter properties it will also not work in a water splitting device.

The above discussed boundary conditions indicate that for reaching highly efficient H_2O splitting PEC devices the PV converter's ${U_{ph}}^{mpp}$ must be larger, but as close as possible to ΔE^{op} (see eqs. 10, 12). However, if the photovoltage ${U_{ph}}^{mpp} = {U_{ph}}^{op}$ produced by the PV converter is much larger compared to the difference ΔE_{H_2O} of the reversible half-cell reaction potentials of $\varepsilon°(H_2O/O_2)$ and $\varepsilon°(H^+/H_2)$, any kinetic limitations of the water splitting reactions can be avoided. The extra potential may help to drive the water splitting reaction even for less effective electrocatalysts but, on the other hand, will reduce the STH efficiency due to the reduced photocurrent. Therefore ${U_{ph}}^{op}$ must be adjusted to gain maximum efficiency: an energy transformation loss results from an increased difference of the operational photovoltage to the thermodynamic potential difference $|\Delta E_{H_2O}| = \varepsilon°(H^+/H_2) - \varepsilon°(H_2O/O_2)$ of 1.23 V, which is equivalent to the energy stored in the H_2 formation (fuel production). This value will not be changed for larger operational photovoltages applied. As a consequence due to the counteracting dependence of photovoltage and photocurrent of the absorber bandgap a higher fundamentally possible photovoltage will lead to a reduced photocurrent and thus to a reduced STH efficiency η_{STH}. As already mentioned above, this behavior is different to an electric power producing PV converter, where both j_{ph} as well as U_{ph} can be used to increase the performance value without lower limits (see eq. 1).

2.3 Promising integrated PV/PEC device structures

There are very many different device structures possible for PV converters and even more for PEC cells especially if multijunction cells are considered (see e.g. [18, 50]), which shall not be discussed in this contribution as their performance should be rather similar from a fundamental idealizing point of view and any advantage or disadvantage of a given structure depends mostly on specific materials' properties. Therefore we will use a p-i-n device structure, most probably as tandem or triple structure, as has been suggested as promising most simple PV device structure for advanced thin film solar cells [32, 51], which would also provide a good basis of an efficient PEC structure (Figure 4). For simplicity we will first discuss only single absorber structures, which are the standard arrangements in Si thin film solar cells [23], and are also used for single crystalline Si

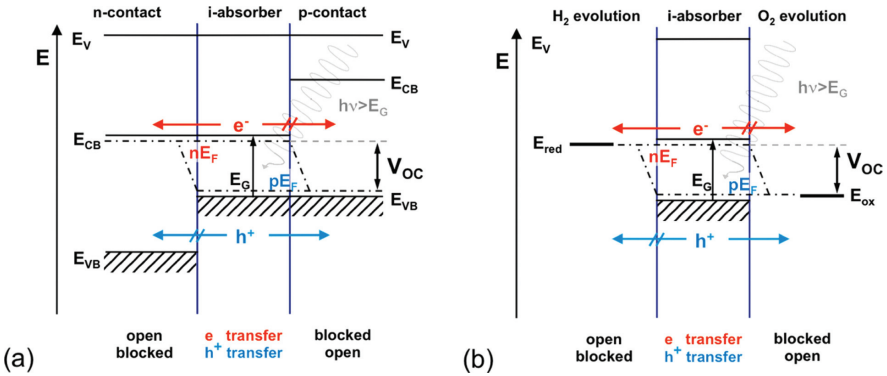

Fig. 4: Schematic idealized representation of an p-i-n PV or p-i-n PEC device structure under illumination (open circuit conditions). In such structures the semiconductor absorber layer is directly connected to either n-doped and p-doped wide bandgap window contact layers (n/p-membranes) (a), or with selective electron and hole transferring electrolyte contacts to be used for the HER and OER water splitting half cell reactions (b). Reprinted by permission from Springer Nature: Springer, *Photoelectrochemical Solar Fuel Production*, S. Gimenez, J. Bisquert (Eds.) ©(2016).

in the so called HIT™cell [52]. The correlation of photovoltaic solid-state cells to photoelectrochemical cells is immediately evident, when the wide band gap metallic conducting TCO contacts are substituted or extended by electrochemical contacts providing the conditions for charge transfer reaction to the electrolyte. We have neglected in these sketches any contribution of overvoltages as we are in quasi-equilibrium conditions ($U = U_{ph}{}^{oc}$). As will be discussed later, the working device structures must be modified in a similar way for PV and PEC applications by adding additional layers, which are needed to electronically passivate and chemically shield the semiconductor/oxide as well as the PV semiconductor/electrolyte contacts. The difference between surface engineered solar cells or surface modified photoelectrochemical cells is only a semantic difference (compare Figure 4).

The advantage of such p-i-n cells is the fact, that naturally doped (intrinsic) absorber layers can be applied without the need of forming highly doped absorber layers. The diffusion voltage (linear or weakly bend space charge layer) is formed between the front (n^+-doped) and back (p^+-doped) wide band gap contacts, which favour a vectorial charge carrier separation. For idealized structures as shown in Figure 4 high theoretical efficiencies can be reached. If we use absorber layers of large absorption coefficients beyond $\alpha > 10^4\ cm^{-1}$, which would be preferential for thin film absorber layers, their thickness d (equivalent to the absorption length L_{ph}) may be strongly reduced to typical values of 1–2 μm (assuring that

$L_{ph} \geq 3/\alpha$). As we need quantum efficiencies of close to 1 all light generated charge carriers must reach the contacts without severe bulk recombination losses. This will be the case if the minority carrier diffusion length given by

$$L_d = (D \cdot \tau)^{1/2} = (k \cdot T/e \cdot \mu \cdot \tau)^{1/2} \tag{14}$$

or the drift length including potential gradients $E = grad\ U$ at the maximum power point given by

$$D_L = \mu \cdot E \cdot \tau \tag{15}$$

with D_L, μ, τ as minority carrier diffusion constant, mobility, and lifetime exceed the thickness d of the absorber layer. In such cases and neglecting any surface (interface) recombination loss the photocurrent of absorbed photons can reach a quantum efficiency of about one.

Essential are proper band energy alignments at the interface between the wide band gap contact material and the light absorbing semiconductor as shown in Figure 4a. The conduction band offset must be close to zero to the n-contact and maximized at the p-doped back contact and vice versa for the valence band and conduction band offset to the doped back contact to minimize voltage losses. Such band offsets help to increase the photovoltage due to reduction of the reverse dark currents which are effected by the large additional barriers $j_0 \propto \exp(-\Phi_B/kT)$ (the barriers Φ_B add up the energy difference of the Fermi level to the respective band edge position plus the additional value of the band discontinuity).

The direct contact to metallic co-catalysts will lead to surface recombination losses and surface Fermi level pinning reducing in general the built-in diffusion voltages, which can only be avoided with adjusted heterocontacts containing electronic passivation layers (see Figure 5) [30]. Similar conditions must be reached for nearly any PEC device: In this case an efficient and fast charge transfer must be possible from the conduction/valence band edge for electron/hole transfer to the electrolyte. Such conditions can only be expected for a high density of states in the electrolyte and a proper alignment of the band edge states to the involved electrolyte and/or co-catalyst energy levels. This will in general only be the case for reversible redox couples and cannot be expected for the multi-electron transfer HER and OER redox reactions, which is the reason that additional co-catalysts are needed for efficient charge transfer. However, these extra catalysts deposited onto the semiconductor do not only provide a catalytic function for controlling the charge transfer reactions, but they also function as contacts to the semiconductor which must be adjusted for avoiding potential losses. For both the PV cell as well as for the PEC cell the interface must be kept (almost) free of surface (interface)

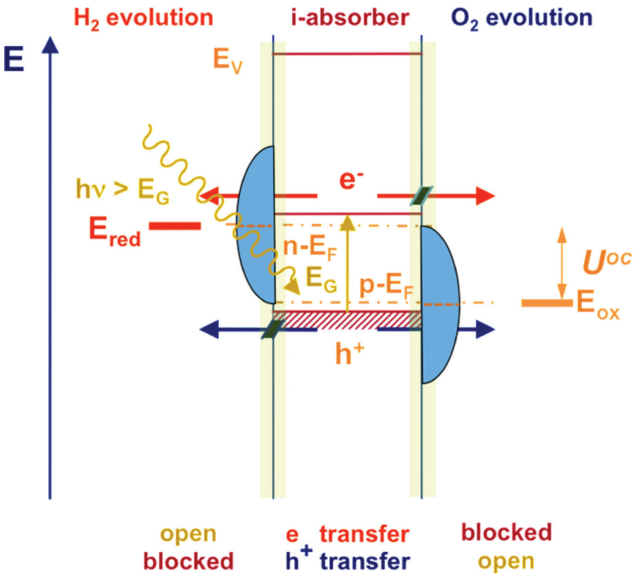

Fig. 5: Schematic representation of the formation of a surface modified PV or PEC device consisting of a highly absorbing semiconductor layer, a surface passivation layer (green) and metallic co-catalysts for HER and OER. Reprinted by permission from Springer Nature: Springer, *Photoelectrochemical Solar Fuel Production*, S. Gimenez, J. Bisquert (Eds.) ©(2016).

states to avoid recombination losses. An efficient passivation of surface states with contact formation are essential requirements for potentially high conversion yields. For PV contacts this favours the application of heterocontacts with wide band gap materials as oxides and disregards directly deposited metals, for a more detailed discussion see [30]. Based on this argumentation a maximum photovoltage close to the semiconductor band gap and approaching the Shockley-Queisser limit can be expected for PV devices with low recombination losses in the bulk and at the interfaces (leading to parallel or shunt resistance $R_p \rightarrow$ infinity) as well as low resistance and loss free charge transfer reactions across the interfaces and fast transport within the semiconductor (leading to a series resistance $R_s \rightarrow 0$):

$$U_{ph} = kT/e \ln(j_{ph}/j_0) \tag{16}$$

For PEC cells with electrolyte contacts similar boundary conditions must be fulfilled. For proper electrolyte contacts the redox potentials of the half-cell reactions must provide comparable contact properties as the idealized TCO membranes as used for the PV converter (Figure 4b). As has been proven by Lewis et al., well defined and specifically designed PEC cells provide rather ideal contact properties when reversible redox couples in organic solutions are used as contact

phases which avoid any reaction of the semiconductor with H_2O [53, 54], which, however, cannot be avoided for water splitting PEC cells. PEC device structures containing electrochemical contacts will provide high primary PV conversion efficiencies in producing maximised photocurrents j_{ph} and photovoltage U_{ph} only in cases when current loss (due to recombination) and voltage loss (owing to misaligned electron states) contacts can be avoided. For PEC cells this means, that only in cases, where fast electron transfer couples with adjusted redox potentials and aligned electrolyte density of states, we may expect high PV conversion efficiencies. Such conditions cannot be expected for PEC water splitting devices. In this case we have to consider instead of reversible redox couple multi-electron transfer reactions, which for H_2O splitting involves the bonding (surface stabilisation) of reactive intermediates to the solid surface. If these intermediates are bound at the right energy levels (close to the conduction band for HER or close to the valence band for OER) is usually not to be expected. If this is not the case and the minority carriers loose part of their electrochemical potential will be evident from shifts of the photocurrent potential onset to the flat band potential measured in the dark. For this reason co-catalysts for achieving an efficient charge transfer reaction must and are usually added to improve performance. However, the deposition of these additional catalysts will also affect the semiconductor/electrolyte contact e.g. by passivating surface states. This dual functionality is probably in operation for most interfaces with an additional catalyst layer, but often has not been thoroughly investigated to identify the specific role of each mechanism. There are a few examples published, where the relative effect of each process was examined [55, 56]. However, detailed experiments combining surface science studies as well as electrochemical characterization procedures are needed to obtain clear results. In most cases additional solid-state layers specifically adjusted for surface/interface engineering are necessary to provide a proper alignment of energy states and potential distribution across these interfaces. The reason is that the electrolyte redox states involved in the charge transfer reaction strongly deviate from the idealised Marcus-Gerischer distribution deduced from reversible one-electron transfer redox couples, as the stabilisation of intermediate reaction products on a catalyst's surface is needed. A more detailed discussion on electronic DOS of electrolytes in relation to charge transfer processes is given in [39, 57]. These additional layers are needed to design an efficient semiconductor/electrolyte contact for multi-electron transfer reactions as used e.g. for water splitting, which consists of at least a passivation layer and an electrocatalyst. These extra layers must be aligned in their electronic coupling to the semiconductor base material as it is shown schematically in Figure 5. It should be noted, that such interface engineered PEC contacts must be specifically designed for every multi-electron transfer PEC cell as e.g. also for CO_2 reduction devices; the specific

aspect is that the needed electroctalysts will be different and thus may also need different intermediate passivation layers. Again, it should be emphasized that the needed interface engineering approaches may as well involve wet chemically formed reaction layers or intermediate layers deposited within or outside an electrochemical cell.

As a consequence of the above given reasons it must be expected that, in general, any efficient PEC device will consist of electronic and chemical passivation layers (in rare cases one layer may provide both duties) and different co-catalyst layers for the HER and OER. It should be mentioned that for metals the width of its electron energy distribution (DOS range with a high density of electron states) will be even broader than for the situation shown in Figure 5, covering an energy width of several eV depending on its electronic character with d-bands DOS widths being much smaller than s or p-bands. As the catalyst must transfer the electrons and holes, respectively, without a loss in photovoltage, its contact properties are defined by its Fermi level position after contact formation. For achieving this, the metal co-catalyst must be aligned in an energetic position as shown in Figure 5 with the HER (OER) catalyst Fermi level position close to the conduction (valence) band edge. How this can be secured for metal catalysts having a priori non-adjusted work functions will be discussed in more detail below.

Following our above given argumentation, two principally different device structures for the photoelectrochemical water splitting application may be considered. One is based on only one single semiconductor absorber material and therefore must use wide bandgap absorbers such as ZnSe, ZnTe, SiC, GaP, GaInP, InGaN etc. (see Figure 6). As all of these semiconductors are not stable in contact to the electrolyte, they must be shielded from the direct contact to the electrolyte by a chemical and electronic passivation layer. The chemical passivation layer must avoid any decomposition reaction due to hole (electron) induced oxidation (reduction) reactions involving the solvent and the semiconductor. In addition, the electronic passivation layer must ensure the passivation of the surface states usually present on all semiconductor surfaces due to the loss of bulk bonding (loss of translational symmetry). These interface layers may be designed according to the modifications discussed below and shown in Figure 6a and b. In most cases these layers are needed to define the position of the Fermi level close to the band edge (conduction band for HER and valence band for OER, respectively) by appropriate doping (buried junction). As these passivation layers usually will not work as electrocatalysts an additional catalytically active (metal) deposit (e.g. Pt for HER or RuO_2/TiO_2 for OER) has to be added to enhance the desired reaction. Note that in this figure we have used the standard presentation of a photoelectrochemical cell as usually found in literature with a bulk semiconductor absorption

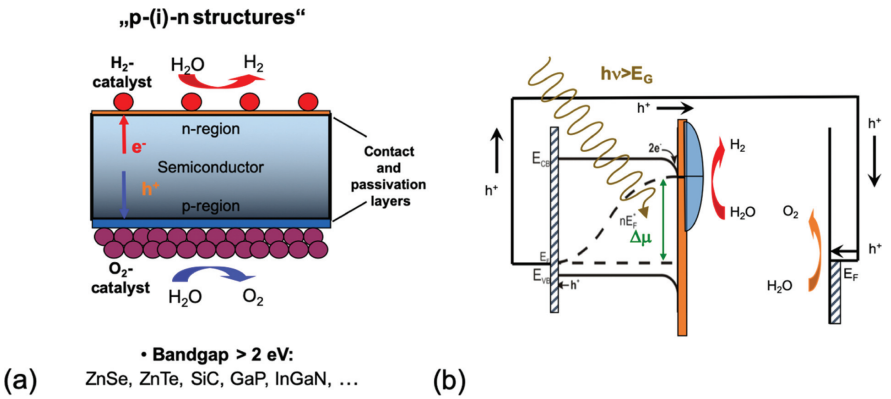

Fig. 6: Schematic structure of a photoelectrochemical solar cell for water splitting (a) being composed of a p-i-n absorber layer with n/p doped surface layers, chemical/and/or electronic passivation layers on front and back sides as well as co-catalysts for HER and OER. (b) Schematic energy band diagram under illumination (approximating flatband conditions) and the needed photovoltage for H_2O splitting given by the splitting of the electron-hole chemical potential (difference of electron and hole quasi-Fermi level) under illumination. Reprinted by permission from Springer Nature: Springer, *Photoelectrochemical Solar Fuel Production*, S. Gimenez, J. Bisquert (Eds.) ©(2016).

layer, where the thickness of the semiconductor substrate is much larger than the absorption length; for this reason the splitting of the quasi Fermi levels is restricted to the thickness of the absorption plus diffusion layer (illumination from the electrolyte side, Gärtner approximation [58]). In dependence of the doping of the semiconductor one may use photocathodes (p-doped substrates) and photoanodes (n-doped semiconductors). From the given examples of applicable semiconductor materials with the right band gap larger than 2.3 eV and sufficient charge carrier mobilities it is clear, that such passivation layers are needed to stabilize the materials from corrosive side reactions. It should be noted however, that none of the many suggested absorber layers have reached photovoltages in the range from 1.6 to 1.9 V until now, which would be required for efficient water splitting. Alternatively, oxides and nitrides with band gaps between 2 and 3 eV have been suggested, which should provide improved stabilities, and for this reason have intensively been investigated in recent years [17, 18]. However, due to their intrinsic bad charge carrier mobilities (hopping transport of polaron states) the performance has not reached a competitive value, yet. In addition, also these materials need passivation and co-catalyst layers to improve their properties. Furthermore, it has been recently found that polaron states limit the photovoltage, which can be used for the induction of the photoelectrochemical reactions [59–62].

As an alternative and to our expectation more promising device structure, we suggest the combination of two or more different absorber materials with significantly different band gaps, which will absorb different parts of the solar spectrum (tandem or multi-junction (absorber) cells). The materials of choice need to fulfil the requirements as defined above for single absorber materials and should have bandgaps at around 1.2 and 2 eV. Whereas a number of semiconductor materials with promising properties may be found for the low bandgap partner, there is only a limited choice for the large bandgap partner up till now. The envisaged tandem structures (see Figure 7) may be arranged as classical two terminal semiconductor tandem solar cells as shown in Figure 7b. Alternatively,

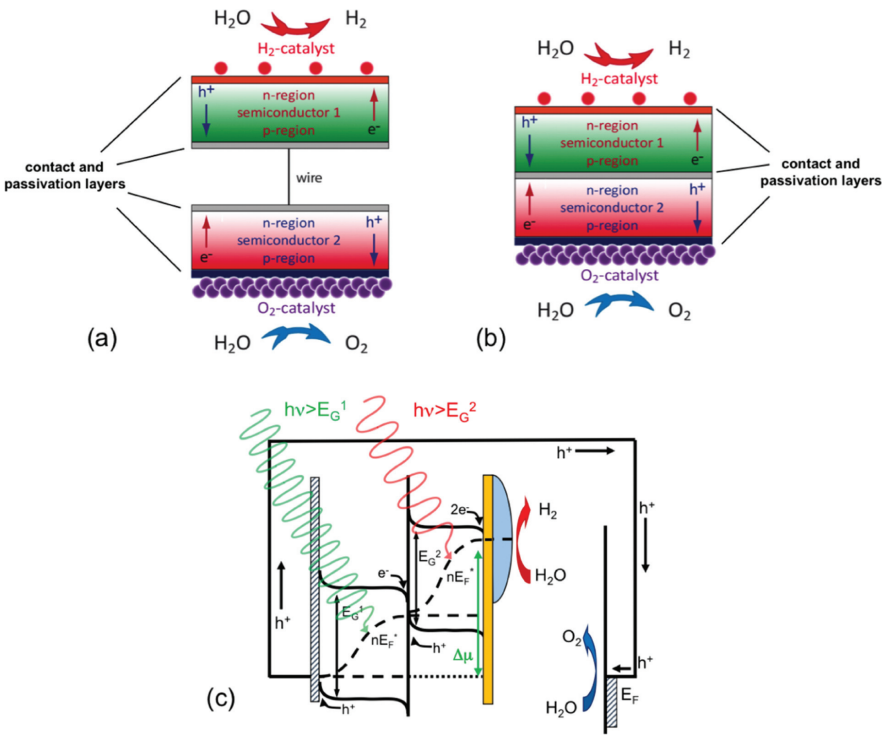

Fig. 7: Schematic structure of a buried junction solar cell used as PEC device either as two independent PV converters (a) or as integrated tandem cells deposited on each other using a tunnel junction for charge carrier recombination ((b), applying p-i-n junctions as shown in Figure 4). (c): Schematic energy band diagram under illumination (approximating flat band conditions) and the needed photovoltage for H_2O splitting as added up from the two solar cell components and given by the splitting of the electron-hole chemical potential (difference of electron and hole quasi-Fermi level) under illumination. Adapted by permission from Springer Nature: Springer, *Photoelectrochemical Solar Fuel Production*, S. Gimenez, J. Bisquert (Eds.) ©(2016).

one may also use two different materials electrically connected to each other and being exposed to the same electrolyte as is shown in Figure 7a. This arrangement is often presented and may be a favourable solution for photoelectrochemical water splitting cells if the integration of the two materials may cause additional problems.

Systems like these, including also triple or quadruple arrangements, have the advantage, that the final photovoltage will be the sum of the two or more coupled PV converter components without losing too much of photocurrent, since photons with different energies (wavelength) will be utilized. This is schematically shown in the energy diagram of Figure 7c. Also, for these tandem structures passivation layers and co-catalysts are needed, which must be designed with the same favourable energy alignments as discussed above for the single absorber layers. As discussed below, tandem solar cells as well as tandem based PEC cells can deliver higher conversion efficiencies. Especially for photoelectrolysis devices, this provides a decisive advantage with respect to possibly available conversion efficiencies as also small band gap semiconductors can be utilized to absorb a major part of the solar spectrum and thus will deliver part of the needed photopotential for the water splitting reaction under illumination. To achieve high efficiencies the two (three, four) semiconductor junctions must be matched to each other across their interfaces by an efficient tunnel junction without losing too much of their difference in minority carrier chemical potential. In addition, the photocurrents from the two (three, four) separate PV junctions must be matched to each other, since the cell with the lowest photocurrent determines the maximum photocurrent reached through the device. These boundary conditions are also true for all other multi-absorber arrangements in which e.g. two photoelectrochemical cells are combined as photoanode and photocathode to the final water splitting device. It is therefore not reasonable to couple PV converters with high photocurrents to low photocurrent PEC converters in a series connection.

Unfortunately, there are only a limited number of investigations on the development of wide band gap absorbers, and also the alternatives for highly efficient low bandgap absorbers are scarce. The only systematically investigated and successfully developed class of materials are 3–5 semiconductors, which also provide the highest PEC efficiencies in multiabsorber cells [63, 64]. But, all the above given arguments how to optimize a specific semiconductor as absorber for PV cells or as PV component in PEC cells can also be transferred to tandem PV or PEC cells. The PV converter part must be optimized in a comparable manner independent of a possible application as electricity producing solar cell or fuel producing photoelectrochemical cell. This argument can also be turned around and simplified to the fact, that only good PV tandem arrangements will also provide competitive PEC tandem arrangements. On top of it the specific design criteria need to

be solved, which are related to the electrochemical reactions: To optimize the multi electron hydrogen and oxygen evolution reactions, specifically designed and adjusted co-catalysts must be included. To stabilize and passivate the semiconductor chemically and electronically, specifically designed wide band gap interlayers must be developed. And finally, to secure a loss free coupling of the co-catalysts to the valence und conduction band states, the electronic interface structure must be tuned in relation to each other.

2.4 Interface engineering to obtain efficient PEC junctions

As is evident from the considerations presented above an efficient PEC device is either based on an already optimized PV device and then modified for the water splitting reactions or is alternatively constructed from promising semiconductor absorber materials and then adjusted as PEC junction with optimized properties: it can be expected that both device structures will look very much the same at the end (see Figure 7). As is well known for Schottky barriers, semiconductor/electrolyte interfaces but also for semiconductor/passivation layer/co-catalyst/electrolyte interfaces active intrinsic surface (formed from dangling bonds) or extrinsic interface states (formed by interaction to the contact phases) may strongly modify the idealized interface energy diagrams as presented in Figure 7c (compare also Figure 4). As deduced from fundamental semiconductor physics, intrinsic surface states exist on the surface of most semiconductors due to the loss of the crystalline translational symmetry (for a more detailed discussion refer to [65]). These states may be situated in the band gap and thus interfere with contact formation and charge transfer. For most covalently bound semiconductors (e.g. Si, GaAs, CdTe) such surface states are related to dangling bonds. They may be situated at different energy positions in the band gap depending on the electronic properties (covalency vs ionicity) and on surface orientation and will be modified by surface relaxation and reconstruction (see e.g. a summary in [66]). However, due to possibly formed interface interactions during contact formation with any contact phase and thus also with the electrolyte, these intrinsic surface states are energetically shifted by chemical bond formation forming extrinsic surface states or interface states. As a consequence the electronic structure of most semiconductor surfaces, as represented by the electronic density of states as well as by the surface potential as a function of Fermi level position, band bending, and work function, will deviate from the bulk as can be easily measured for UHV processed surfaces. After being exposed to ambient conditions or to the electrolyte further changes will occur, which need to be investigated inside the electrolyte or at least after the exposure to possible reactants. Finally, solid state phases deposited being either of metallic or semiconducting

nature are forming hetero contacts and will further change the contact properties [38, 65, 67–71]. Depending on the details of the interface interactions, where in most cases chemical reactions are involved, the surface (interface) properties may be designed (engineered) for reaching proper contact potential distributions and electron transfer reactions. Surface science techniques have been used to elucidate the microscopic details of semiconductor junction formation and to determine the decisive factors governing the contact properties (see e.g. [30, 39]. For a schematic representation of the expected modification of interfacial contact layers compare Figure 8. In general, a semiconductor/electrolyte interface without exposing modified electronic properties will not exist in contact to the electrolyte, maybe with the exception of layered MX_2 semiconductors [40] or chemically passivated semiconductors [72]. But also for such at first sight ideal semiconductor/electrolyte junctions containing chemically saturated inert surfaces, the need of catalyzing the multi electron transfer reactions of the HER and OER, respectively, requires active surface reaction sites, which must be provided by the co-catalyst. These catalytic surface reaction centers, in general, will modify the underlaying layers. As a consequence, one may either deduce a "chemical" molecular surface design of a PEC junction providing a SC/X-R-Y/Z-M_{cat} sequence of chemical layers with strong bonding groups X, Y, Z (R: organic sidechains) for electronic and chemical surface passivation and for bond formation to the M_{cat} co-catalyst. Alternatively, one may choose a solid-state approach with a SC/MO/M_{cat} sequence of solid layers, which have to provide the identical duties. How many different layers will be needed or if layers must be substituted by other compounds (e.g. oxides as MO vs. other compositions MX) depends on the details of bonding

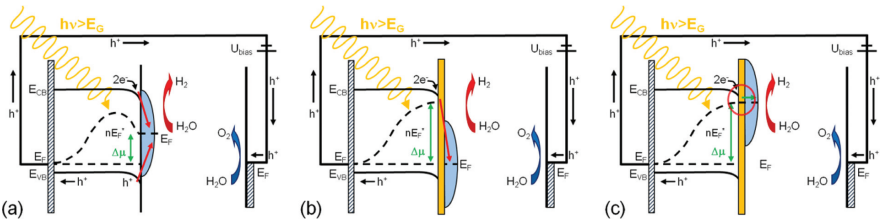

Fig. 8: Different SC/co-catalyst layers as used for PEC HER. a) Direct deposition of the metal catalyst onto the semiconductor showing Fermi level pinning. As a consequence the photovoltage is small and the photocurrent at the MPP will be reduced by surface recombination. b) Deposition of the metal co-catalyst onto an insulating wide band gap passivation layer. As a consequence a MOS/MIS junction is formed, which will lead to a complete diminishement of the photovoltage inside the SC by electron transfer to high workfunction catalysts. c) Ideally designed MOS/MIS layer with a degenerately doped contact layer (n^+ Oxide, n^+ SC (l) layer). The metallic co-catalyst aligns to its Fermi level and the high photovoltage of the device can be used.

interaction and the band energy alignment across the interface. This is also true for a chemical set of passivation layers. These considerations indicate, that the design of a specifically adjusted "interphase" will be needed for every efficiently working device. The considerable complexity in structure and composition may be further changed by the involved interface chemistry and physics. The research effort to design and engineer the interfaces of semiconductor junctions is one of the challenging research directions in the optimization of thin film solar cells and plays a comparable decisive role in PEC junctions.

The experimental and theoretical understanding of such complex hetero interfaces (e.g. SC/electronic passivation layer/(chemical passivation layer)/co-catalysts/electrolyte) needed for PEC applications is still not given. Even for individual interfaces (e.g. SC/oxide or SC/metal) the electronic properties depend on surface orientation, pretreatment and processing of the specific junction. For this reason, a number of different theoretical models are still being discussed in the literature to account for the experimental facts regarding non-ideal Schottky barrier heights (Fermi level pinning) to be expected for SC/co-catalyst interfaces [39]. Similar theories have been developed for the hetero interface as it forms between the absorbing low band gap semiconductor and the wide band gap hetero-contact (see e.g. Refs. [38, 65]). In general, it cannot be expected that such hetero interfaces are free of detrimental electronic interface states especially when lattice mismatched and chemically dissimilar materials are combined. In most working solar cell devices either homo junctions (Si) or interdiffused graded heterocontacts (CIGS, CdTe) provide reasonable interface properties [51, 73]. In a similar way surface (interface) states are also expected to be formed at semiconductor/electrolyte contacts. Due to the large number of possible reactants, the chemical nature of possibly formed surface states and their surface density of states distribution is mostly unknown.

An extensive discussion on the formation and properties of surface and interface states as given by the the intrinsic (distribution of dangling bonds or open coordination sites) or extrinsic (band gap interface related states induced by the contact phases) surface/interface electronic structure of semiconductors is out of the scope of this paper. But, because of the severe effects in contact formation (Fermi level pinning) as well as for charge transfer (recombination and mediated charge transfer) induced by additional bandgap states at phase boundaries some general considerations shall be presented, because they are essential for interface engineering. Especially for numerous of the novel semiconductors studied in PEC devices no elaborate theoretical or experimental surface studies do exist, which would allow to deduce their surface/interface electronic properties. Therefore, only some qualitative conclusions are possible:

1. Generally, most (all) semiconductors will initially form a high concentration of intrinsic surface states when the bulk translational symmetry is lost. These states depend on the surface orientation, which determines the bonding geometry of the involved surface atoms and will usually be influenced by surface relaxation and reconstruction.
2. The type and character of surface states depend on the bulk bonding of the parent semiconductor. Shockley states are formed due to dangling bonds of covalently bound semiconductors. Tamm states are due to unsaturated ionic surface atoms with dominant ionic bonding. Semiconducting transition metal compounds form new states due to a change in their coordination sphere.
3. The initially present intrinsic surface states will be modified by chemical bond formation or surface interaction with contact phases. As a consequence extrinsic surface states or interface states may be formed. Contact phases may lead to the passivation (shift of surface states out of the bandgap) or induction of new states into the bandgap.
4. These surface/interface states take part in contact formation; band bending can be induced or removed depending on the Fermi level position in the bulk determined by semiconductor doping concentrations and the surface/interface DOS and their electron occupation, defined by the surface neutrality level (formally equivalent to a surface state Fermi level position before equilibrium formation).
5. The concentration of surface/interface states may be very high (one to several electronic states per surface atom translating to surface concentrations of 10^{14} to 10^{15} cm^{-2}); if they are active they will lead to Fermi level pinning at their charge neutrality level and in dependence on their energetic positions to enhanced surface recombination or loss of photopotential in charge transfer.
6. Transient surface states may also be formed in the course of multi electron charge transfer reactions, when intermediates are strongly bound to the electrode's surface and the involved charge transfer reactions are slow.
7. Due to the interaction with contact phases, surface states can be electronically passivated (shifted outside the bulk band gap). In this case they will not interfere with contact formation and charge transfer. If due to contact formation new energetic positions will be reached, these states may be strongly interfering with the charge carrier distribution in the dark and under illumination.

Many research efforts in semiconductor (opto)electronics are directed towards a better understanding of surface/interface effects as they may dominate the (opto)electronic properties. The rationale design of interface composition and interface electronic structure are efficient measures for electronic passivation or controlled engineering of surface/interface states; the aim is to shift them to an

energy range which is favorable for contact formation and which allows to control the involved electron transfer reactions into the right directions. In order to get additional insights of the involvement and character of surface/interface states surface science studies may provide appropriate means ([74] and articles therein).

It is evident that for any efficient PEC device the interface properties must be also adjusted for securing the maximum photovoltage of the PV converter by minimized surface recombination and electronically aligned electron transfer reactions. From the photocurrent voltage curves provided in literature it is obvious, that this has not been reached for most junctions as shifts in the photocurrent onset and transient current spikes usually show up. An optimal engineered hetero interface will show current voltage curves and conversion efficiencies approaching those of ideal semiconductor junctions.

One important further difference of semiconductor/electrolyte contacts e.g. compared to semiconductor/metal contacts should be emphasized. In solid state contacts usually the positions of the interface DOS are fixed and only the occupation will change with contact formation (formation of band bending) according to Fermi statistics or under illumination according to the distribution of quasi Fermi levels. For semiconductor/electrolyte contacts also the density of surface states may change, as certain defect levels (surface states) may be formed by surface corrosion reactions induced by voltage or illumination thresholds. As photocorrosive decomposition reactions of semiconductors under illumination are in most cases multistep electron-transfer reactions, the intermediates may form different new surface species with modified energy density of states distributions of transient surface species with electron occupations not in equilibrium with bulk states, which in turn will change the electric potential distribution across the interface. This eventual instability of surface conditions is more severe considering surface/interface reactions of semiconductor/electrolyte contacts. It may even be expected to be generally occurring if charge transfer reactions are considered which need strong interfacial bonding for electrocatalytically demanding reactions as HER and even more for OER. This will be different for solid-state junctions (Schottky barriers), where generally only the occupation of given electronic interface states may be considered (rigid surface band structure approach). The problem of dynamic Fermi level pinning involving transport of charges and reactants from and to the semiconductor surfaces is thus a general problem for low charge transfer kinetics and needs specific experimental tools for analysis [36].

The H_2O redox reaction steps can only be realized without large energy loss, if formed intermediates are stabilized by the interaction with the solid surface. Possibly formed intermediate states, which are energetically or kinetically unfavorable, will therefore lead to an undesired formation, occupation and side reactions of surface/interface states. As a consequence, the photoelectrochemical

cells show bad performance. Proper interface engineering strategies to modify the active semiconductor junction in contact to the electrolyte must be developed to improve the performance of the water splitting device. If the desired interface engineering can be better performed by wet surface treatments within the electrolyte junctions or if the needed contact layers are prepared before as specifically developed contacts, this strategy should be decided in dependence on the performance of the overall device. In the latter case knowledge and optimization strategies of solid-state semiconductor junction applies. Whenever the surface photovoltage is strongly reduced compared to the expectation for a good semiconductor or when recombination and/or charge trapping kinetics is evident from photocurrent transients due to high concentrations of surface/interface states an electronic passivation layer is needed, which shifts the unfavorable surface states out of the band gap region by chemical bond formation. Dynamic charging effects of interface or band gap states may shift the energetic position of a specific solid state component in the layer sequence in relation to other components [75]. Therefore, a proper energetic alignment of all energy levels involved in the charge transfer sequence across the junction during the photoelectrochemical HER or OER reaction will be essential for obtaining high conversion efficiencies. This shall be exemplified for the hydrogen evolution reaction for a p-semiconductor/passivation layer/co-catalyst/electrolyte junction with perfect passivation properties, which will not be negatively affected by the involvement of semiconductor interface states. In Figure 8 we show the band energy diagram, which would be expected for a p-semiconductor (Si) junction for HER; we assume that a bulk Pt layer is used as H_2 evolving catalyst. Note that for such considerations the energy diagrams must be sketched close to the MPP representing the working conditions. Band energy diagrams showing short circuit conditions with the original existing band bending in the dark should not be applied as no photovoltages have been built up (short circuit condition). Without any passivation layer the Pt directly deposited onto Si will lead to pinning, expected close to midgap, and about half of the photovoltage will be immediately lost. In addition, the related high surface recombination velocity will lead to reduced photocurrents. Such Fermi level pinning effects will be mostly independent of the metal for most classical semiconductors with covalent bonding properties [38, 39, 65]. For a passivated surface using a non-doped and thin insulating layer (e.g. a thin SiO_2 perfect passivation layer) the high work function of Pt would lead to a position of the metal Fermi level close to the valence band edge of the semiconductor. Such junctions are called MIS or MOS devices and can be treated with the well-known Cowley-Sze model [76]. As a consequence of the non-aligned electron states the photovoltage built-up in the semiconductor would be completely lost, as the electrons from the conduction band will be transferred to the low-lying Pt Fermi level

position, which is situated close in energy to the semiconductor valence band edge (Figure 8b). Thus, the usable photovoltage obtained with active HER catalysts consisting of noble metals with high work functions will be small at the MPP even if the photocurrent reached under strong reverse bias may be high. This loss is in contrast to the chemical expectations but is an effect of semiconductor physics in contact formation. Applying lower work function metals (e.g. Ag or Cu) will not solve the problem as the gain in photovoltage due to the upward shift of their Fermi level position will be counterbalanced by bad HER overpotentials. This unfavorable situation can only be avoided, if the passivation layer(s) also works as a contact layer. For this purpose, a low work function wide band gap contact of an highly conductive TCO layers as SnO_2, TiO_2 etc. may be used. Also, a highly doped n^+ Si surface layer can be applied to define the junction. In these cases, the energy-converting junction with large band bending is built up at the p-SC/TCO contact interface. If the doping level in the first contact layer to the semiconductor is high enough, the high work function catalyst will align to the Fermi level of this n^+-TCO or n^+-Si contact layer with no or small potential losses. As a consequence, the electron transfer will occur close to the energy level of the conduction band edge. Therefore, the overall device structure is basically a PV solid state solar cell contact inserted into an electrolyte solution. In this device the inner layer forms a buried junction, which defines the energetic conditions of the PV converter and thus the operative photovoltage, whereas the outer surface layer involving the co-catalyst forms the electrolyzer component of the device which will not disturb contact formation, as it will align to the n^+-oxide (Si) Fermi level and will just lead to low overpotentials for the electrochemical reactions. Such buried junctions to passivation layers evidently characterize the envisaged interface design of any efficient PEC electrolyte junction, where the deposited co-catalyst is aligned to the Fermi level of the highly conductive n^+ passivation layer. This may be a TCO or degenerately doped SC-layer of low work function. For these conditions the co-catalyst layer and its energy states involved in electron transfer will not lead to voltage losses.

As a consequence of these considerations, the buried junction may be rather complex. It consists at first of an electronic passivation and/or contact layer to the semiconductor, which must define good PV converter properties due to the formation of high diffusion voltages. The next layer may be an appropriate chemical passivation layer before the co-catalyst for HER and OER is added. These layers shall prevent surface corrosion and enhance the desired H_2O redox reactions. This sequence of layers must be adjusted in a way that the HER catalyst is aligned close to the conduction band edge and for a photoanode the OER catalyst close to the valence band edge of the PV component. These are the conditions needed to avoid losses of photopotential to allow for the electron (hole) transfer close

to the conduction (valence) band edge at operation voltage under illumination. How many different layers are needed and which sequence will provide the best performance must be checked for every case as some layers may provide several functions at the same time.

It should be mentioned at this stage, that most direct semiconductor electrolyte contacts which have been modified by co-catalysts or additional layers, which may be formed outside the electrolyte by the deposition of additional layers or inside the electrolyte by potential cycling experiments, most probably also form such buried junction interfaces if their performance is approaching the desired positive values. However, in many cases the interface properties have not been analyzed yet sufficiently to allow such conclusions.

3 Examples of highly efficient photoelectrochemical cells

3.1 Buried junction multiabsorber cells

As already discussed above, the photovoltage needed for bias-free water splitting varies with the used catalysts. The photocurrent reached at the required voltage determines the solar-to-hydrogen device efficiency (see eq. 12). For an efficient device it is therefore essential to identify and develop solar cells, which provide an adjusted large voltage ($U_{ph}{}^{oc}$ and U_{MPP}) range in combination with high photocurrents. So far there are only a limited number of multi-junction PV cells available which can be tuned according to the PEC needs for water splitting. Besides the different 3–5 semiconductors, which are very expensive, the high photovoltage/high photocurrent tradeoff can be solved by multijunction solar cells made of amorphous (a-Si:H) and microcrystalline (μc-Si:H) silicon which we have chosen as working examples. But at first we want to present in a short survey multiabsorber cells which have been realized so far with meaningful conversion efficiencies.

3.2 Development of Si thin film solar cells for photoelectrochemical water splitting

The exploration of multi-junction photovoltaic cells made from silicon for photoelectrochemical water splitting has been around for more than 20 years now [77–85]. They can be used in a wired or wireless (artificial leaf) arrangement and are comprised in most cases by two or more active thin film silicon (a-Si:H, μc-Si:H) or silicon alloy layers. The solar to hydrogen conversion efficiencies are

reported of being below eight percent. In 2011 a triple cell based on thin film silicon was presented by Reece et al. reaching a total efficiency for hydrogen production between 2.5% and 4.7% [26].

In our attempts we started our research work in using multi-junction thin film Si solar cells as photocathode. The details on the experimental development of the multi-junction PV cells and the integration into advanced photoelectrosynthetic cells will be described in another paper within this issue [86]. In this part we will just shortly discuss the design criteria for the experimental realization to the theoretical concepts discussed in Section 2 of this paper.

Combinations of a-Si:H and μc-Si:H allow for a more precise adjustment of the PV parameters and suffer less from stability issues under prolonged illumination (Staebler-Wronski effect) [87] compared to their all-amorphous counterparts. In the following sections of our contribution, we will demonstrate how multijunction solar cells of thin film silicon can be applied as photocathodes in an integrated PV-EC device.

3.2.1 Performance of Si thin film multi-junction cells

The typical solar to electric power conversion efficiency performance of different multijunction solar cells using thin film Si cells are presented in Figure 9. A maximum efficiency of nearly 14% can be reached [88]. The figure also shows how increased values in photovoltages are detrimental to the maximum photocurrent, which can be achieved. In remembrance of the discussion of the possible solar-to-H_2 efficiency (Section 2.) the important boundary condition is to reach an operative photovoltage $U_{\mathrm{ph}}{}^{\mathrm{op}} > 1.6$ V of the maximum power point; the photocurrent reached at this point will determine the maximum solar-to-hydrogen efficiency.

a-Si:H and μc-Si:H absorber layers were implemented in multi-junction solar cells. It was found, that the $U_{\mathrm{ph}}{}^{\mathrm{oc}}$ of these solar cells can be tuned in both large (600 mV) and small (50 mV) steps from 1.5 V to 2.8 V in $U_{\mathrm{ph}}{}^{\mathrm{oc}}$ and from 2.3 V to 2.3 V in U_{MPP} without significantly impairing the device efficiency. Figure 10 displays the achieved $U_{\mathrm{ph}}{}^{\mathrm{oc}}$ as a function of the j^{sc} of the developed single and multi-junction solar cells. As a consequence, our development routes allow us to tune the $U_{ph}{}^{\mathrm{oc}}$ of the photovoltaic cells over a wide range while keeping the device efficiency above 11% for the multijunction solar cells. The highest efficiency in combination with a high $U_{ph}{}^{\mathrm{oc}}$ of 2.3 V was achieved with the a-Si:H/a-Si:H/μc-Si:H triple junction solar cells, which exhibited a solar to electric efficiency of 13.6%. Also Figure 10 nicely shows the effect of the $U_{\mathrm{ph}}{}^{\mathrm{oc}} - j^{\mathrm{sc}}$ tradeoff of thin film silicon solar cells.

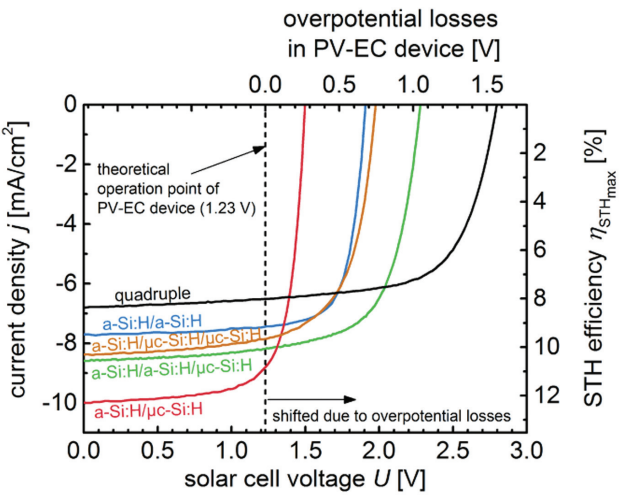

Fig. 9: Illustration of the achievable solar-to-hydrogen efficiency η_{STHmax} in PV-EC devices for water splitting based on thin film silicon solar cells (adapted from [35, 89]). The illuminated *j-V* curves of tandem, triple, and quadruple junction solar cells are linked with the theoretical operation point of a PV-EC device at 1.23 V (dashed vertical line, without overpotential losses). In real PV-EC devices this operation point is shifted due to overpotential losses, which are plotted on the upper x-axis. The right y-axis depicts the achievable STH efficiency as a function of the respective photocurrent density at a certain overpotential multiplied by the value of 1.23.

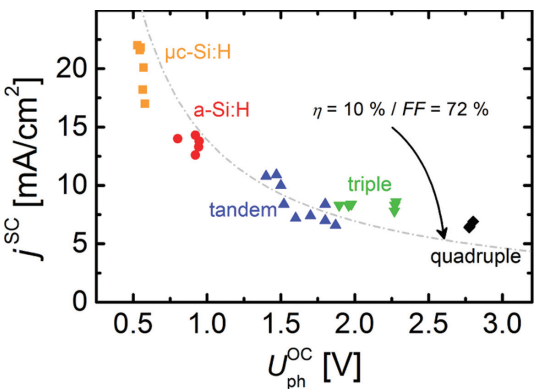

Fig. 10: Open circuit voltages $U_{ph}{}^{OC}$ as a function of the short-circuit photocurrent densities j^{sc} of the developed a-Si:H and µc-Si:H based single and multi-junction solar cells. The grey dotted line indicates a photovoltaic efficiency η_{PV} of 10% assuming a FF of 72% (adapted from Refs. [35, 89]).

It should be noted that the conversion efficiencies of the multi-junction solar cells presented in our study are very close to the highest efficiencies reported for solar cells made of thin film silicon of 13.4% [90]. These high efficiencies of our high-voltage cells have been realized by a careful adjustment of the individual sub cell current densities. It is important to "match" the photocurrent densities, i.e. to equally distribute the total current among the sub cells in a multi-junction solar cell in order to avoid current limitation. We matched our cells with respect to the photocurrent by integrating microcrystalline silicon oxide [91, 92] as doped intermediate reflecting layers and by adjusting the thicknesses of the sub cell absorber layers [87]. The current matching was evaluated by means of quantum efficiency measurements.

The ability to vary the photovoltaic parameters over a wider range, as presented in Figure 9, to adjust the needed photovoltages provided by the PV converter component to the needs of the electrolyzer component of the integrated cell is a very helpful design advantage for photo-electro-synthetic cells. Depending on the particular requirements of various PV-EC systems, which may combine different co-catalysts for the HER or OER with different overpotential losses, the PV component can be chosen to fulfil the different voltage requirements for bias free water splitting. Figure 9 illustrates the range of overpotential losses which may be possible for different PV-EC devices based on the developed multi-junction solar cells. The illuminated *j-V* curves of the developed tandem, triple and quadruple junction solar cells are plotted and linked to the theoretical operation point of a PV-EC device. The PV-EC device operates in its operational photovoltage value with maximized efficiencies when both electrodes are connected to each other in a two-electrode arrangement without adding extra bias potentials e.g. via a potentiostat. As a reference point indicating an ideal system without overpotential losses, the PV-EC device would operate at a voltage of 1.23 V of the solar cell, indicated by a straight vertical dashed line in Figure 9.

In real systems overpotential losses lead to a shift of the operation point towards more positive bias. The photocurrent density j_{op} at this required photovoltage ${U_{ph}}^{oc}$ can be used to estimate the maximum STH efficiency η_{STHmax} (under the assumption of 100% faradaic efficiency) of the PV-EC device. Assuming that all PV parameters of the solar cells remain unchanged when they are integrated in a PV-EC device, the current voltage curve of the PV component and its maximum power point allows, in considering any additional shift induced by voltage losses of the electrochemical cells, to predict the performance of PV-EC devices based on the integration of the different developed solar cell arrangements with appropriate integrated electrocatalysts (see Figure 2). The validity of these assumptions can be checked by comparing the current voltage curves of the solar cell with the current voltage curve of the electrolyzer arrangement to each other. Strong

deviations of the ideal curves to the measurements of the real PV-EL system will indicate additional losses in the device, which may be either due to interface losses due to device integration or additional resistance losses within the circuit e.g. due to membranes or electrolyte resistance. The maximum STH efficiency which can be expected when using different multicrystalline/amorphous Si thin film multijunction cells can be deduced from Figure 9 from the operation point line at the respective overpotential from the upper x-axis. As can be deduced from this figure, a-Si:H/μc-Si:H tandem junction could provide a maximum STH efficiency over 10% when the PV-EC device would operate without any overpotential losses. When considering losses, triple and quadruple junction photocathodes are needed for a working device. These results indicate that different multi-junction Si thin film solar cells can be prepared based on the combination of μc-Si and a-Si absorber layers. Based on a maximum solar-to-electricity efficiency of such cells we may expect a maximum of STH efficiency of about 10% when the realized photocurrents are considered.

3.3 Buried PV-EC water splitting cells based on thin film Si

When the thin film silicon solar cell is setup as a PV-EC, it becomes the photoactive part of a buried-junction photoelectrode (compare Figure 11). The separation of the light induced charge carriers and the generation of the photovoltage is located far away from the electrolyte interface. Therefore, the photovoltaic characteristics of the solar cell are not altered, when the cell is used as a photoelectrode (buried junction approach). Between the photoactive silicon layers and the electrolyte a contact layer is inserted, which acts also as a protection layer against corrosion. In our case the solar cell is covered with a highly reflective Ag back contact layer for the photovoltaic characterization without electrolyte. In a buried-junction electrode the Ag layer would have to act in addition as the buffer layer. Usually the buffer layer material exhibits high overpotential for the chemical reaction. In this term Ag is also not a good catalyst for the water splitting reaction. A common strategy to increase the performance of a buried junction electrode is to add a catalyst onto the buffer layer (i.e. Pt) to enhance the chemical reaction. Because the thin film solar cell, the buffer layer and the catalyst is arranged in series, the current flowing through all layers (components) is equal. Hence the buried junction electrode can be understood as a series connection of the separate characteristics of its components. Given that the resistivity of the Ag contact can be neglected, the photoelectrochemical characteristic of our system can be predicted by the photovoltaic performance of the solar cell (PV) and the electrocatalytic properties of the applied catalyst [34, 93], compare Figure 2.

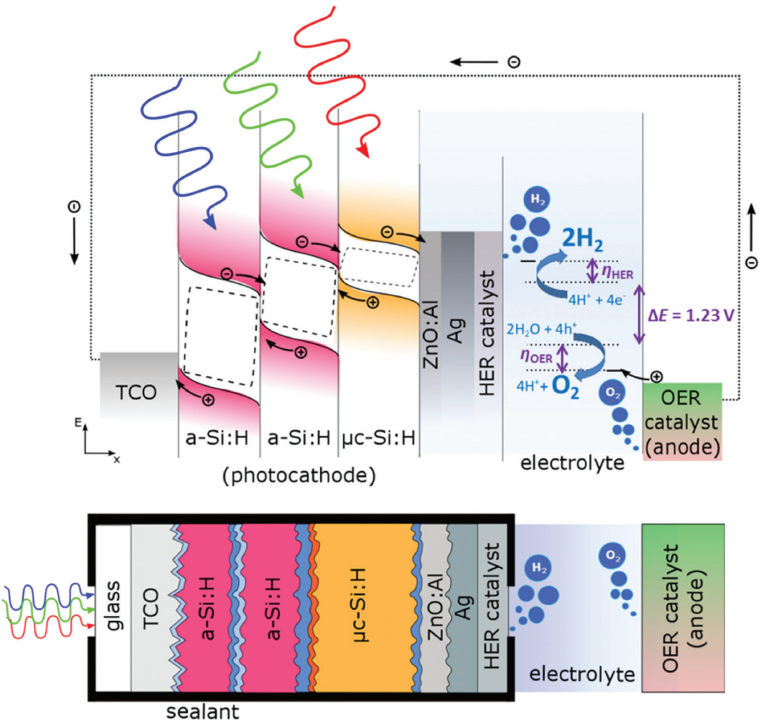

Fig. 11: Schematic of a buried triple junction electrode. The electrode is composed of a photoactive part (the thin film silicon solar cell), buffer layer (Ag) and an electrocatalyst for the chemical reaction (Pt). The cell is completed by the addition of an anode with an efficient OER catalyst material (adapted from [35]).

To investigate the complete PV-EC device characteristics, two-electrode arrangements have to be employed and are presented in this section. Figure 12 depicts the voltammograms in two-electrode configuration of the real PV-EC devices based on the developed multi-junction solar cells (see Figure 9). The measurements were performed in 0.1 M KOH and Pt was used as HER catalyst layer (approx. 150 nm) on top of the solar cell Ag contacts.

The shape of the curves is different from the pure solar cell *j-U* presented in Figure 9. In particular the FF and U_{ph}^{op} are reduced, mainly because of the electrolyte resistance and the overpotential losses at the electrode surfaces (Pt and RuO_2), respectively. The modeling of the photocurrent-voltage characteristics was presented elsewhere [34] (see Figure 2). The saturation photocurrent is slightly reduced compared with the pure *j-U* measurement on the solar cells, because for the PV-EC measurements no anti-reflection foil was used. As could be predicted from Figure 9, the measurement shown in Figure 12 confirms that the photovoltage

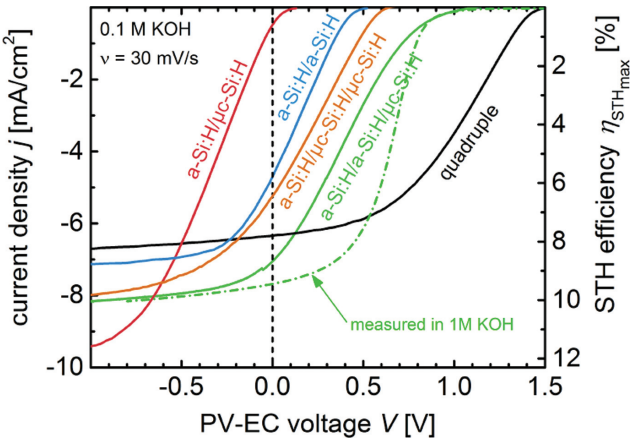

Fig. 12: Linear sweep voltammetry measurements of the PV-EC devices based on thin film silicon multi-junction photocathodes with a 150 nm thick Pt layer as HER catalyst on top of the Ag contact and a RuO_2 counter electrode for the OER reaction. The measurements were performed in 0.1 M KOH at a scan rate of 30 mV/s. The right y-axis depicts the achievable STH efficiency as a function of the photocurrent density at 0 V applied bias multiplied by the value of 1.23. Figure adapted from Refs. [35, 89].

generated by the a-Si:H/μc-Si:H tandem photocathode is not sufficient to operate the constructed PV-EL device in its maximum power point (MPP) under real operating conditions. This is very unfortunate as the device provides the highest J^{sc} of all investigated solar cell types (see Figure 9). But when this PV device is coupled to the co-catalyst to be used as PV-EL system the additional losses within the circuit (mostly the overvoltage losses) only allow its operation at a j^{op} of 0.5 mA/cm^2. This result supports the previously given estimation that an effective photovoltage ${U_{ph}}^{op}$ of 1.5 V is the minimum output voltage required to run this specific PV-EC device (Pt and RuO_2 as HER and OER catalyst, respectively, and 0.1 M KOH electrolyte solution) bias-free in an efficient manner. For the a-Si:H/μc-Si:H solar cell this value is hardly reached. For the a-Si:H/a-Si:H based device the operation point is still not at its maximum power point but in the current slope of its voltammogram, thus an increased photocurrent is found with j^{op} of 4.8 mA/cm^2, but it is not reaching the possible maximum value of about 7 mA/cm^2. Although the a-Si:H/μc-Si:H/μc-Si:H triple junction devices provides a higher ${U_{ph}}^{oc}$, and consequently a higher $E_{onset,cat}$ (as apparent from Figure 12), the j^{op} is not increased compared to the a-Si:H/a-Si:H tandem cells. Evidently for this device additional further improvements in the fill factor must be realized in order to reach the MPP photocurrent under short-circuit condition, and thus, to achieve a higher STH efficiency. The highest operation photocurrent density j^{op} is provided by the

a-Si:H/a-Si:H/μc-Si:H based PV-EC device. The device operates close to its MPP at 7.1 mA/cm^2, which corresponds to an estimated STH efficiency of 8.7%. This STH conversion value can be further increased when this device is operated in 1 M KOH electrolyte to reduce the electrolyzer related losses even further. As a consequence an even higher operation photocurrent density is achieved and the device is able to provide an estimated STH efficiency of 9.5%. This is to our knowledge the highest STH conversion value which has ever been reported for cheap thin film based artificial leaf devices. Alternatively, one may also consider the performance of a quadruple junction device. This device provides a lower photocurrent in its plateau region of 6.3 mA/cm^2 with a corresponding 7.6% STH efficiency of lower value with the same catalysts used. But as the j^{op} of this device is found in the flat region of the voltammogram (current plateau region) this device provides a rather large excess photovoltage, which could be used in choosing other non-precious catalyst materials for the HER and OER, respectively. In summary these examples show how the device performance of PV-EL systems can be deduced and realized based on the knowledge of the current voltage curves of the components. The advantage of using thin film Si devices is that the PV and the electrolyzer performance can be adjusted to each other within certain limits.

3.4 Interface engineering of thin film PV-EC cells

3.4.1 Stabilization of the photoelectrodes with a TiO_2 buffer layer

Alternatively, to the up to now considered configuration one may envisage a specifically designed interface architecture in combining layers for contact formation with layers for chemical passivation on the photocathode. An improved stability of the photoelectrodes can be achieved by substituting the Ag back contact with an oxidic buffer layer. In contrast to silver an oxide exhibits a stronger bonding to silicon semiconductors. TiO_2 is well known for its chemical stability in aqueous electrolytes and provides the required protection of the tandem cell against corrosion [94]. Due to oxygen vacancies TiO_2 is intrinsically n-doped and supplies a high conductivity for electrons, which is required for the HER [95]. The TiO_2 buffer layer is in this case prepared by reactive magnetron sputtering from a metallic Ti target onto the previously etched a-Si:H/a-Si:H tandem solar cells. The Pt catalyst is deposited via an electrochemical route from a 0.5 M H_2SO_4 + 0.5 mM K_2PtCl_4 solution. After deposition (−0.5 mA/cm^2 for 20 min), Pt particles with diameters up to 200 nm are formed on the photoelectrode with the TiO_2 buffer layer (see Figure 13).

These electrodes exhibit an improved stability during HER visible by the almost constant potential while evolving hydrogen at −0.5 mA/cm^2. In Figure 14a

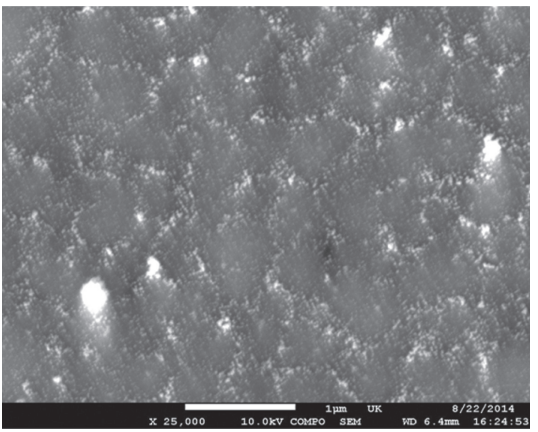

Fig. 13: Scanning electron microscopy image of a-Si:H/a-Si:H/TiO_2 photoelectrodes after Pt deposition. An overlay of the secondary and the back-scattered electrons was used to generate the image. The white bar at the bottom of the figure corresponds to an one micrometer length. Figure adapted from [96].

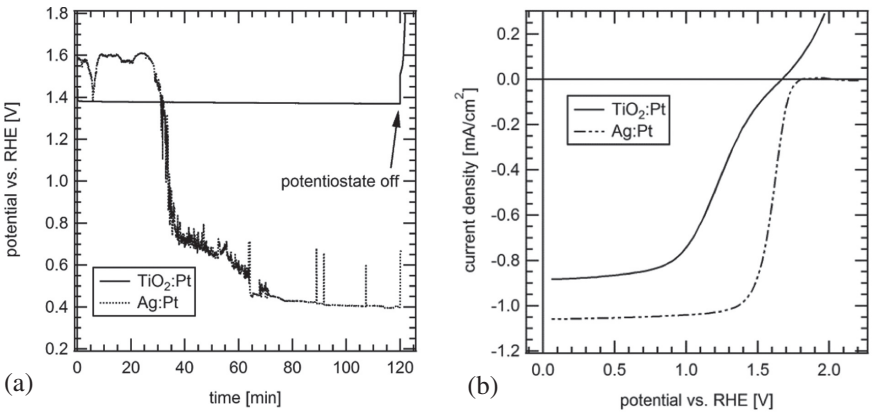

Fig. 14: (a) Potentiometric measurement of a-Si:H/a-Si:H/TiO_2 at -0.5 mA/cm^2 in 0.5 M H_2SO_4. (b) Linear scan voltammetry of a-Si:H/a-Si:H photoelectrodes with TiO_2 and Ag contact/buffer layer and Pt in 0.5 M H_2SO_4. Both graphs were obtained under illumination with a white light LED (10 mW/cm^2). Figures adapted from [96].

a comparison between a photoelectrode with Ag contact and one with TiO_2 buffer layer is depicted. The TiO_2 sample suffers a reduction in photovoltage and current (see Figure 14b). When measuring the resistive potential drop for a titania layer at a current density of 1 mA/cm^2 a potential loss of only 4 mV is encountered. Hence, the reduction of the photovoltage does not originate from the resistivity of

the thin TiO_2, but has to be assigned to the interface property between the tandem cell and the buffer layer.

To get an insight into the charge transfer properties of the a-Si:H/TiO_2 contact, interface experiments were performed by subsequently depositing TiO_2 onto the a-Si:H/a-Si:H tandem cell and XPS analysis after each step. The spectra are displayed in Figure 15 after different deposition times. At the beginning of the experiment the Si surface of the tandem solar cell is visible. The Si 2p signal is composed of the amorphous silicon and an oxygen component at higher binding energy, which is assigned to a SiO_2 surface layer. From both Si 2p components a SiO_2 layer thickness of 1.3 nm can be extracted before the deposition of the TiO_2 starts [97]. The contribution of the oxide layer is also visible in the O 1s spectrum. Upon deposition the Ti 2p emission and a second O 1s species at lower binding energy shows up, which is attributed to TiO_2. Further deposition subsequently reduces the silicon components and increases the TiO_2 signals. Additionally an increasing SiO_2 layer thickness can be observed. The topmost spectrum in Figure 15 shows the sample after electrochemical deposition of Pt onto the TiO_2 buffer layer. It contains an asymmetric Pt 4f line indicating the metallic properties of the Pt catalyst. The position of the valence band of a-Si:H and TiO_2 can be monitored from the relative positions of the respective core lines as well as from the valence band spectra. The absolute positions of the core lines are affected by the photovoltage of the tandem cell device during XPS analysis, induced by the XPS source and caused by a low lateral conductivity of the a-Si:H/TiO_2 layer structure [30, 98, 99]. The small shift of the spectrum in the topmost spectrum can be explained by a changed photovoltage due to the Pt deposition.

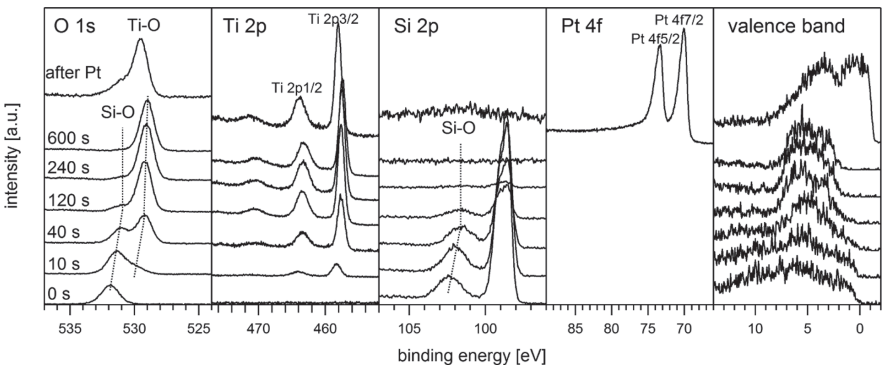

Fig. 15: XPS spectra of an a-Si:H/a-Si:H solar cell after subsequent deposition of TiO_2 (adapted from [96], for more information see [100]). The total deposition time of TiO is indicated in the O 1s spectra. The XPS spectrum of the a-Si:H/a-Si:H solar cell after Pt deposition is shown in the top row. All lines are shifted due to surface photovoltage effects [30, 98, 99].

From the photoelectron spectra given in Figure 15a a band energy diagram can be constructed for dark conditions, which gives information about the energy alignment of the energy bands across the $Si/SiO_2/TiO_2/Pt$ interface. As is theoretically expected (see Section 2.3) the Pt Fermi level is adjusted to the Fermi level of the highly n-doped TiO_2 passivation layer. The Pt catalyst forms an ohmic contact to the TiO_2 buffer layer. Therefore, no potential loss can be expected at this interface. Also the junction is mostly defined by the space charge layer induced by the n-doped TiO_2 layer. However, the diffusion voltage as well as the charge transfer properties are strongly governed by defect states within an intermediate SiO_2 reaction layer (see Figure 16). The interface between a-Si:H and TiO_2 exhibits only a small conduction band offset, which is negative for electrons traveling from the tandem cell into the buffer layer. Hence, the principle band line-up of the TiO_2 to Si used for the tandem solar cell arrangement seems to allow a favourable alignment of conduction band states, which was also observed on model interfaces with crystalline silicon [101]. Unfortunately, the electron barrier induced by SiO_2, which can be identified at the interface, leads to deviations from the ideal junction behaviour: The SiO_2 interface layer on the a-Si:H reaches a thickness of >2 nm at

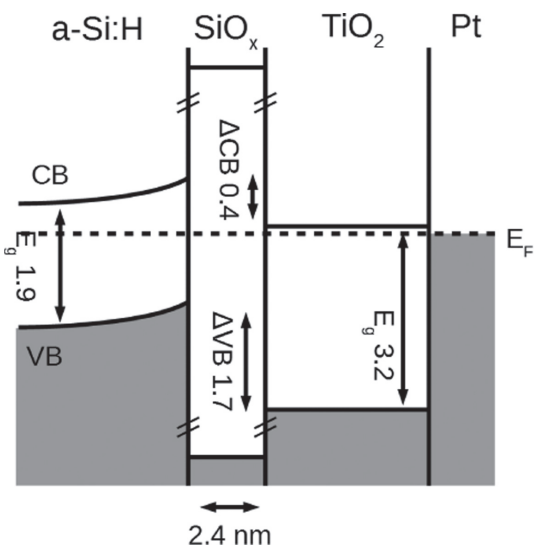

Fig. 16: Band alignment in the dark of the interface between an a-Si:H/a-Si:H solar cell, TiO_2 and Pt on the basis of core line positions of the XPS measurements. Indicated values are in eV. The conduction band minimum (CB), the valence band maximum (VB), the band gaps (E_G) and the Fermi level (E_F) are shown. The conduction band offset (ΔCB) and the valence band offset (ΔVB) is indicated between a-Si:H and the TiO_2 buffer layer. Adapted from [96], for more details see [103].

the end of the deposition using ALD, which is made responsible for the reduced photovoltage of the electrodes with TiO_2. Due to the high thickness a tunnel process through this layer is unlikely and the charge transfer is hindered [102]. In further optimisation steps the oxide layer has to be reduced to improve the photoelectrochemical performance. This interface layer is one clearly proven example of the case where also an internal double layer potential drop $\Delta\Phi$ lead to a loss of usable photovoltage (see Section 2).

One strategy to reduce the SiO_2 thickness is the application of chemical etching to remove the native oxide on the silicon tandem solar cell before the deposition of the TiO_2 buffer layer. The XPS spectra after three pretreatment recipes are depicted in Figure 17a. After etching the tandem solar cell in 50 wt% KOH (2 min) a distinct signal remains in the Si 2p region originating from a 1.6 nm thick SiO_2 layer. An extended treatment in 1 M HCl and 50 wt% KOH (each 2 min) leads to a slight reduction of the oxide layer to 1.1 nm. A further reduction of the thickness can be achieved by an etching procedure with NH_4F (1 M HCl 2 min and 40 wt% NH_4F 5 min). This treatment reduces the SiO_2 layer almost completely before the TiO_2 deposition (0.1 nm). Afterwards the TiO_2 buffer layer as well as the Pt catalyst were deposited and electrochemically characterized in 0.5 M H_2SO_4 (see Figure 17b). Despite the significantly different amount of oxide at the beginning of the TiO_2 deposition the impact on photoelectrochemical behaviour is small. Only the sample etched in KOH, with a much thicker oxide layer, shows a reduction in photovoltage. The other pre-treatments lead to a similar performance. Unfortunately, the complete removal of the SiOx layer does not restore the performance

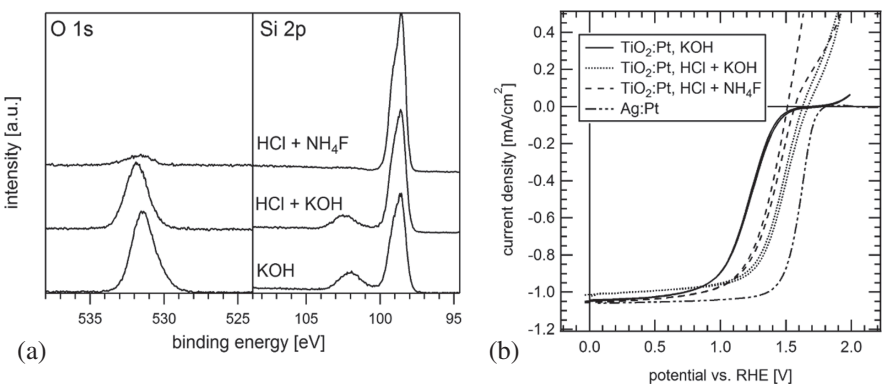

Fig. 17: (a) XPS detail spectra of Si 2p emission of pretreated a-Si:H/a-Si:H tandem solar cells before TiO_2 deposition. (b) Cyclic voltammograms of these photoelectrodes after TiO_2 and Pt deposition in 0.5 M H_2SO_4 under illumination with a white light LED (10 mW/cm^2). Figures adapted from [96].

shown by the photoelectrodes with Ag back contact. One possible reason may be that during sputter deposition the interfacial oxide grows, making the initial thickness insignificant.

An adjustment of the oxygen partial pressure in the sputter atmosphere is one approach to prevent the oxide formation during the TiO_2 deposition. An oxygen amount of 4% in the sputter atmosphere results in a strongly reduced photovoltage of the tandem cell electrode (see Figure 18). As the oxygen amount is lowered the photoelectrochemical curve is shifted to anodic potentials. A photovoltage almost equal to the photoelectrode with Ag back contact can be achieved with 1.5% oxygen in the sputter atmosphere. Consequently, the optimization of the deposition parameters of TiO_2 is a key to reduce the silicon oxide formation and to improve the performance of these photoelectrodes. The growth of the silicon oxide interfacial layer is only possible, when the TiO_2 deposit is not thick enough to prevent the oxidation of the silicon beneath. Therefore, the adjustment of the oxygen partial pressure at the beginning of the deposition is sufficient to prevent the SiO_2 formation. A metallic Ti interface layer between Si and TiO_2 was investigated by Seger et al. [104, 105]. With this strategy they achieved good contact properties for their crystalline silicon photoelectrodes. A detailed study of the a-Si:H/Ti/TiO_2 has to be conducted to clarify, if this strategy can be adapted for amorphous silicon photoelectrodes.

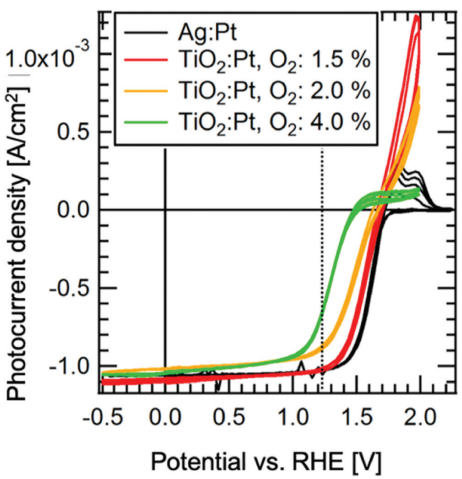

Fig. 18: Cyclic voltammograms of a-Si:H/a-Si:H photoelectrodes with TiO_2 and Pt in 0.5 M H_2SO_4 under illumination with a white light LED (10 mW/cm^2). The TiO_2 buffer layers are deposited with different gas atmospheres containing 1.5, 2 and 4% O_2. Figure adapted from [96].

3.4.2 Optimization of catalysts

Besides a good buffer layer an optimized catalyst is also necessary to achieve a high solar to hydrogen efficiency. Such a catalyst must show a long-term stable adhesion to the buffer layer and a high activity. Enlarging the active area can easily increase the activity itself. It is therefore desirable to deposit these catalysts with a large surface area but reduced overall weight (mass activity). Also the process must be "soft" in order to avoid damaging the supporting tandem cell.

As catalyst material we continued to use platinum. However, the deposition technique was switched to a chemical vapour deposition (CVD) process. By employing CVD a good adhesion to the TiO_2 can be guaranteed. Furthermore, this synthesis technique enables the deposition of 3D structures with a high surface area and thus with a low overvoltage.

Catalysts were prepared from a platinum (II) acetylacetonate precursor. Layers were deposited on titanium foil covered with a native oxide. As reactive gas, to decompose the precursor, hydrogen and oxygen were assessed. The reactive gas has a major impact on the deposition process. Whereas in oxygen atmosphere the platinum grows as a film on the substrate, in hydrogen the spherical particles were deposited. Here it was concluded that nucleation already starts within the gas phase, facilitating their spherical appearance. In Figure 19 a comparison between the achievable morphologies is shown. The preparation technique and detailed results have been published in a separate report [106]. It is especially noteworthy, that the deposition in hydrogen is possible at temperatures as low as

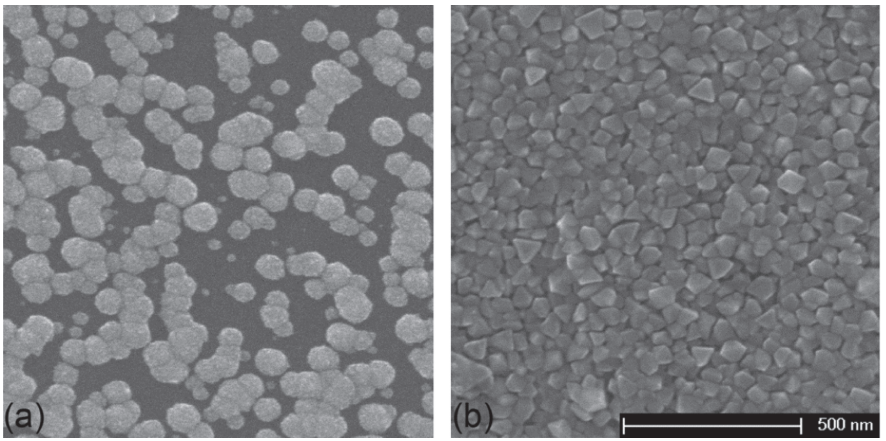

Fig. 19: (a) Pt clusters synthesized in H_2 atmosphere at 150 °C substrate temperature and (b) a platinum film deposited in O_2 atmosphere at 400 °C. Both images have the same scale. Figures adapted from [107], see also [106].

150 °C. At this temperature the a-Si:H/μ-Si:H tandem cells are still stable, whereas the deposition under oxygen atmosphere requires at least temperatures of about 300 °C.

In Figure 20 the overvoltage for the HER in dependence of the ratio between active and geometric surface area is shown. Values for the active area were determined by cyclic voltammetry in the hydrogen underpotential deposition regime, related to hydrogen adsorption onto the Pt surfaces [108] (The reference value used for our calculation is 145 μC/cm^2 for one monolayer of hydrogen on Pt(111) [109]. As can be seen the overvoltage decreases with increasing active area to about 40 mV. In the semi-logarithmic plot even a linear correlation can be identified, as would be expected when a simplified Butler-Volmer current-voltage characteristic can be assumed (eq. 4). Beginning at about R = 10, any increase in surface area does not lead to an improvement of the overvoltage. Hence, there is the optimum point in terms of mass activity.

To assess the quality of the distinctive deposition techniques, Figure 21 shows a comparison between three differently prepared electrodes. In all cases they have not been specifically treated additionally. Furthermore, they show a less steep current slope than freshly prepared and cleaned single crystal electrodes [111]. Clearly, the high surface area of the CVD prepared catalyst leads to an increased activity. The overvoltage has a direct impact on the performance of the photo-electrochemical cell, hence the optimisation of the catalyst with regard to active surface as well as mass activity is of utmost importance. In addition, also the

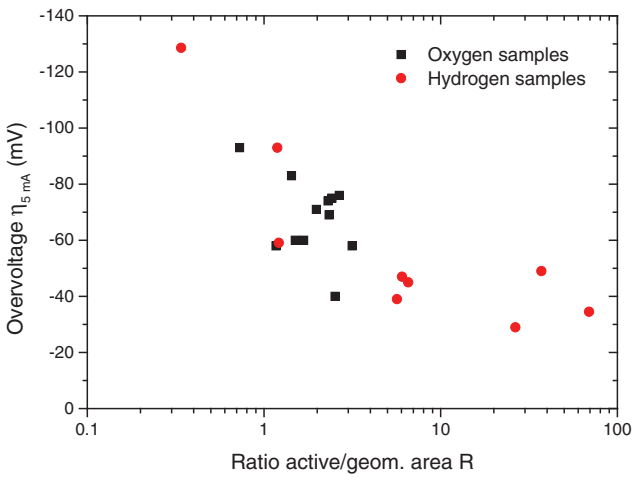

Fig. 20: Correlation between HER overvoltage and the active area. At R = 1 the geometric area matches the active area. Figure adapted from [110], see also [106].

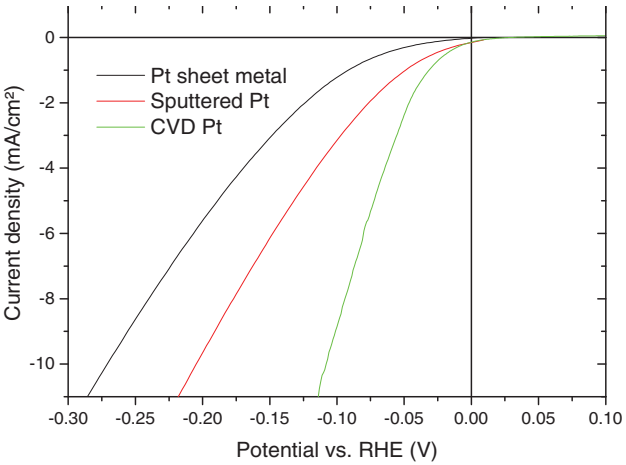

Fig. 21: Current-voltage characteristics of three cathodes prepared by different techniques. The high surface area platinum (CVD) shows the steepest current onset. Figure adapted from [110].

coupling of the catalyst to the buffer layer will be decisive. Fortunately, the high n-type charge carrier density in TiO_2 enables an Ohmic contact to the platinum catalyst despite their large difference in work function.

Further information and results especially on multi junction device stability, interface layer optimisation as well as optimized and more abundant catalyst materials are given in our other contributions [86, 112–115] within this special issue of "Zeitschrift für Physikalische Chemie" and are therefore not repeated here.

4 Summary and conclusions

In this review we have shortly summarized in Section 2 our view on the design architecture of artificial leaves, which in our case are based on inorganic semiconductor absorbers (for a more detailed elaboration please refer to an extended review [30]). In the second part of our contribution in Section 3 we have summarized the prototypical results, obtained in recent years applying thin film Si multiabsorber cells to support our view on the need to use buried junction photo-electrochemical cells (PV-EC devices) for efficient devices.

It can be deduced from fundamental considerations of the involved semiconductor physics and water oxidation and reduction electrochemistry that for working arrangements the PV component and the electrolyser must be connected in series. The working photoelectrochemical cell most probable corresponds in all working devices to a buried PV cell exposed to the electrolyte. There may be cases

where this buried junction is formed within the electrochemical cells by reactions of the semiconductor surface with the electrolyte, but we are not aware of any surface modified non-semiconductor/electrolyte contacts, which lead to efficient devices. Bias free water splitting with competitive conversion efficiencies will only be possible if the performance of the PV component provides the photovoltage needed to drive the oxygen and the hydrogen evolution reaction as given by their electrochemical potentials and in addition provides sufficient voltage to overcome additional losses due to the respective overpotentials and other possible series resistances or internal and external double layer potential drops within the circuit. Adding up these relevant potential differences leads to a minimum open circuit photovoltage of about 1.9 V; this value is higher than the usually discussed value of about 1.5–1.6 V as the difference of U_{ph}^{oc} to the operation voltage of the PEC U_{ph}^{op} cell is often not considered. To reach reasonable photocurrents the open circuit photovoltage U_{ph}^{oc} is of no sense as here the current is 0; the operational photovoltage of the integrated cell U_{ph}^{op} must be close to the photovoltage of the solar converter component at its maximum power point U_{ph}^{MPP}, which is often not considered in studies on photoelectrochemical cells. From such considerations it is clear, that only multijunction cells or a combination of photoanodes and photocathodes will provide high enough photovoltages to reach reasonable conversion yields for light induced H_2 evolution by H_2O splitting.

Working devices need specific surface engineering steps to transfer the electron-hole chemical potential difference produced in the PV absorber under illumination to the electrolyte. First of all, the absorber cell needs contacts, which allow to obtain the maximum photovoltage possible. These contact layers will usually not be equivalent to the co-catalysts deposited in addition for reducing the electrochemical overpotentials due to non-adjusted contact properties. For example, Pt as good HER electrocatalyst is not an appropriate contact layer for p-doped semiconductor surfaces to be used for HER because of its high work function. In general, electronic passivation layers are needed to avoid Fermi level pinning, which may be or may not be equivalent to the contact layer and to the chemical passivation layer, depending on the materials involved. Consequently each layer applied and possibly formed at the junctions must be checked with respect to its contribution to the interface functionality, which is to be achieved.

The solar to H_2 STH conversion efficiency is basically given only by the photocurrent density, which flows at the operation photovoltage point of the current voltage curve. This value must be reached without a potentiostat or bias voltage in a two-electrode arrangement. From this boundary condition it is immediately clear, that the photovoltage onset must be situated more positive than the reversible O_2 evolution potential (ROE) for photocathodes or more negative than the reversible O_2 evolution potential (RHE) for photoanodes; in cases where the

photoelectrode does not provide the needed operational photovoltage for water splitting and the onset of photocurrent is found in between the RHE and the ROE, respectively, only a partial contribution to the overall needed water dissociation potential is provided by the photoelectrode. Especially worse are cases, when the photocurrents are considered at a potential more negative of the RHE for photocathodes and more positive of the ROE for photoanodes, as in these cases no photovoltage is used for providing the needed light induced energy gain for water splitting. The photocurrent density at $U_{ph}{}^{op}$ (being situated outside RHE or ROE) must reach values as defined by the bandgap of the absorber(s) and the reached quantum efficiencies of the PV device. In rather ideal cases this photocurrent is nearly identical to the photocurrent measured in the respective PV cell. From these considerations the possibly reached STH conversion yields can be estimated by adding up the current-voltage curves of the PV component and of the electrolyser component. These can be measured at first independently from each other and then, if the basic data allow their combination, can be realized in an integrated device. If no other additional losses are induced due to the integration, the current voltage behaviour of the integrated PV-EL system should come close to the theoretically added curves as has been show for our Si based devices. This argumentation may be turned around: if the PV component of the photoelectrochemical cell cannot deliver high photocurrents and the needed photovoltages, one cannot expect working or competitive PEC devices for water splitting either. If one is interested in any limitation given by the bulk properties of the used semiconductors or by the contacts forming the energy converting junctions, the performance of regenerative PEC cells with reversible and fast redox couples can be checked in preliminary experiments before specific interface engineering steps related to the integration of co-catalysts and to the severe limitations associated with the water splitting reaction are started.

As is evident from the results on multijunction thin film Si solar cells as presented in the second part of our contribution, the PV component must be adjusted to the conditions of the PV-EC cell to realize the highest performance, which may be possible with a given system. As we could show with our studies the overall performance indeed follows the expected series connection of the components when mostly loss free integration steps could be realized. However, in other cases we have also seen additional unexpected losses e.g. in the photocurrent onset (reduced photopotentials). These are often found when additional chemical stabilisation layers have been added to the devices by extra deposition procedures which have not yet been optimized. These extra losses can be related to additional series resistances in the cell e.g. due to weakly conducting interfacial layers or double layer potential drops across intermediate layers in the device or high series resistances in the electrolyte. So far we have reached an overall maximum

STH efficiency of 9.5% with triple cells made of a-SiH/a-Si/μc-Si, which is the highest value obtained so far with a low cost absorber material. These values were reached by applying so far expensive noble metals as co-catalysts [116]. But as was also shown, if quadruple cells are used with higher photovoltages, even non-noble metals can be applied as electrocatalysts. Additionally, the stability of these devices is still an issue, but can be improved by stabilizing passivation layers as e.g. TiO_2, which on the other hand unfortunately lead to a reduction of performance due to intermediate formed SiO_2 layers.

It should be noted, however, that multijunction cells based on 3–5 epitaxial films still provide higher performance values (see Introduction and ref. [63]). If these high efficiency cells, which are extremely expensive and rather small in size, provide a technologically more promising solution is still a matter of discussion. However, with both approaches it has been proven that STH efficiencies above 10% are feasible. Overall, these results can be taken as promising proof of concepts for direct light induced water splitting and that the production of a storable solar fuel by direct conversion of light energy in an artificial leaf approach will be feasible. There are still a number of novel absorber materials available, which may be developed for efficient thin film tandem or triple solar cells. The promising expectations of reaching higher solar conversion efficiencies by applying the different third generation photovoltaic concepts as suggested by [117] and [23] have not been realized so far, but we do not see any principle hurdles for developing new multi-absorber cells, which require the identification and research on novel wide band gap thin film absorbers to be coupled with known or novel low band gap absorbers. Also improved catalysts avoiding or minimizing the use of noble metal catalysts as well as using highly porous catalyst layers may reduce overvoltage demands and may help to apply low photovoltage devices. Given the significance of the challenge, which must be solved soon to overcome the threats of the energy transition, the needed research money is well spent. The route to a competitively produced fuel from solar radiation seems given; we just need the determination to follow it.

Acknowledgements: The authors acknowledge the valuable contributions of a number of coworkers, who are cited in the respective references, for this report. Financial support was provided by the German Science Foundation in the framework of the priority programme 1613 on Solar Fuels (JA 859/26-1 und JA 859/26-2). In addition, part of our research as cited in our references was supported by the BMBF within a consortium organized by Evonik Industries. W.J. and B.K. are members of the Excellency Graduate School of the German Science Foundation (DFG GSC 1070) “Energy Science and Engineering”.

References

1. C. A. Grimes, O. K. Varghese, S. Ranjan, Light, Water, Hydrogen, Springer, New York (2008).
2. K. Rajeshwar, R. McConnell, S. Licht eds., Solar Hydrogen Generation, Springer, New York (2008).
3. S. Ould Amrouche, D. Rekioua, T. Rekioua, S. Bacha,Int. J. Hydrogen Energ. **41** (2016) 20914.
4. N. S. Lewis, D. G. Nocera, PNAS **103** (2006) 15729.
5. N. S. Lewis, MRS Bull. **32** (2007) 808.
6. J. O. Bockris, Energy: The Solar – Hydrogen Alternative, John Wiley & Sons, New York (1976).
7. J. M. Thomas, W. J. Thomas, Principles and Practice of Heterogeneous Catalysis, VCH, Weinheim (1997).
8. W. Leitner, Angew. Chem. **107** (1995) 2391.
9. K. P. Brooks, J. Hu, H. Zhu, R. J. Kee, Chem. Eng. Sci. **62** (2007) 1161.
10. K. R. Thampi, J. Kiwi, M. Gratzel, Nature **327** (1987) 506.
11. G. A. Olah, A. Goeppert, G. K. S. Prakash, Beyond Oil and Gas: The Methanol Economy, Wiley-VCH, Weinheim (2006).
12. R. G. Lemus, J. M. M. Duart, Int. J. Hydrog. Energy **35** (2010) 3929.
13. Enertrag. https://www.enertrag.com/ (2019).
14. Kopernikus – Power to X. www.kopernikus-projekte.de/projekte/power-to-x/ (2019).
15. A. Fujishima, K. Honda, Nature **238** (1972) 37.
16. D. G. Nocera, Acc. Chem. Res. **45** (2012) 767.
17. K. Sivula, R. van de Krol, Nat. Rev. Mater. **1** (2016) 15010.
18. T. Yao, X. An, H. Han, J. Q. Chen, C. Li, Adv. Energy Mater. **8** (2018) 1800210.
19. A. Heller, R. G. Vadimsky, Phys. Rev. Lett. **46** (1981) 1153.
20. H. J. Lewerenz, C. Heine, K. Skorupska, N. Szabo, T. Hannappel, T. Vo-Dinh, S. A. Campbell, H. W. Klemm, A. G. Munoz, Energy Environ. Sci. **3** (2010) 748.
21. O. Khaselev, J. A. Turner, Science **280** (1998) 425.
22. H.-J. Lewerenz, H. Jungblut, Photovaltaik, Springer, Berlin (1995).
23. A. Luque, S. Hegedus (Eds.): Handbook of Photovoltaic Science and Engineering, Wiley, Chichester (2011).
24. M. A. Green, E. D. Dunlop, D. H. Levi, J. Hohl-Ebinger, M. Yoshita, A. W. Y. Ho-Baillie, Prog. Photovolt. **27** (2019) 565.
25. S. Licht, B. Wang, S. Mukerji, T. Soga, M. Umeno, H. Tributsch, J. Phys. Chem. B **104** (2000) 8920.
26. S. Y. Reece, J. A. Hamel, K. Sung, T. D. Jarvi, A. J. Esswein, J. J. H. Pijpers, D. G. Nocera, Science **334** (2011) 645.
27. Z. Chen, H. N. Dinh, W. Miller, Photoelectrochemical Water Splitting, Springer, New York (2013).
28. A. C. Nielander, M. R. Shaner, K. M. Papadantonakis, S. A. Francis, N. S. Lewis, Energy Environ. Sci. **8** (2015) 16.
29. I. D. Sharp, H. A. Atwater, H.-J. Lewerenz (Eds.): Integrated Solar Fuels Generators, Royal Society of Chemistry, Croydon (2019).

30. W. Jaegermann, B. Kaiser, J. Ziegler, J. Klett, In: Interface Engineering of Semiconductor Electrodes for Photoelectrochemical Water Splitting: Application of Surface Characterization with Photoelectron Spectroscopy in Photoelectrochemical Solar Fuel Production: From Basic Principles to Advanced Devices, S. Giménez, J. Bisquert, (Eds.). Springer International Publishing, Cham (2016), P. 199. doi: 10.1007/978-3-319-29641-8_5.
31. B. Parkinson, J. Turner, In: The Potential Contribution of Photoelectrochemistry in the Global Energy Future in Photoelectrochemical Water Splitting, H.-J. Lewerenz, L. Peter (Eds.). Royal Society of Chemistry, Cambridge (2013), P. 1.
32. P. Würfel, Physics of Solar Cells: From Basic Principles to Advanced Concepts, Wiley-VCH, Weinheim (2009).
33. J. O. M. Bockris, A. K. N. Reddy, M. Gamboa-Aldeco, Modern Electrochemistry – Fundamentals of Electrodics, Kluwer, New York (2002).
34. F. Urbain, V. Smirnov, J.-P. Becker, U. Rau, J. Ziegler, B. Kaiser, W. Jaegermann, F. Finger, Sol. Energy Mat. Sol. Cells **140** (2015) 275.
35. F. Urbain, Light Induced Water Splitting Using Multijunction Thin Film Silicon Solar Cells, Forschungszentrum Jülich, Jülich (2016).
36. L. Peter, In: Kinetics and Mechanisms of Light-Driven Reactions at Semiconductor Electrodes: Principles and Techniques in Photoelectrochemical Water Splitting: Materials, Processes and Architectures, H.-J. Lewerenz, L. Peter, (Eds.). Royal Soc. Chem., Cambridge (2013), P. 19.
37. S. Haussener, C. Xiang, J. M. Spurgeon, S. Ardo, N. S. Lewis, A. Z. Weber, Energy Environ. Sci. **5** (2012) 9922.
38. W. Mönch, Semiconductor Surfaces and Interfaces, Springer Verlag, Heidelberg (1993).
39. W. Jaegermann, In: The Semiconductor/Electrolyte Interface: A Surface Science Approach in Modern Aspects of Electrochemistry, R. E. White (Eds.). Plenum Press, New York (1996), Vol. 30, P. 1.
40. W. Jaegermann, H. Tributsch, Prog. Surf. Sci. **29** (1988) 1.
41. D. Meissner, R. Memming, In: Unpinning of Energy Bands in PEC Cells: A Consequence of Surface Chemistry and Surface Charge in Photocatalytic Production of Energy-rich Compounds, G. Grassi, D. O. Hall (Eds.). Elsevier, London (1988), P. 138.
42. C. Sinn, D. Meissner, R. Memming, J. Electrochem. Soc. **137** (1990) 168.
43. H. M. Kühne, H. Tributsch, J. Electroanal. Chem. Interf. Electr. **201** (1986) 263.
44. J. Schefold, H. M. Kühne, J. Electroana. Chem. Interf. Electr. **300** (1991) 211.
45. M. T. Mayer, Curr. Opin. Electrochem. **2** (2017) 104.
46. S. Hu, C. Xiang, S. Haussener, A. D. Berger, N. S. Lewis, Energy Environ. Sci. **6** (2013) 2984.
47. M. M. May, H. Döscher, J. A. Turner, High-efficiency Water Splitting Systems in Integrated Solar Fuel Generators, The Royal Society of Chemistry (2019), P. 454.
48. K. T. Fountaine, H. J. Lewerenz, H. A. Atwater, Nat. Commun. **7** (2016) 13706.
49. J. R. Bolton, S. J. Strickler, J. S. Connolly, Nature **316** (1985) 495.
50. R. V. D. Krol, M. Grätzel (Eds.): Photoelectrochemical Hydrogen Production, Springer, New York (2012).
51. W. Jaegermann, A. Klein, T. Mayer, Adv. Mat. **21** (2009) 4196.
52. T. Mishima, M. Taguchi, H. Sakata, E. Maruyama, Sol. Energy Mat. Sol. Cells **95** (2011) 18.
53. M. L. Rosenbluth, N. S. Lewis, J. Am. Chem. Soc. **108** (1986) 4689.
54. J. L. Abrahams, L. G. Casagrande, M. D. Rosenblum, M. L. Rosenbluth, P. G. Santangelo, B. J. Tufts, N. S. Lewis, New J. Chem. **11** (1987) 157.

55. C. Zachäus, F. F. Abdi, L. M. Peter, R. van de Krol, Chem. Sci. **8** (2017) 3712.
56. F. Bozheyev, K. Harbauer, C. Zahn, D. Friedrich, K. Ellmer, Sci. Rep. **7** (2017) 16003.
57. R. Memming, Semiconductor Electrochemistry, Wiley-VCH, Weinheim (2001).
58. W. W. Gärtner, Phys. Rev. **116** (1959) 84.
59. C. Lohaus, A. Klein, W. Jaegermann, Nat. Commun. **9** (2018) 4309.
60. C. A. Mesa, L. Francàs, K. R. Yang, P. Garrido-Barros, E. Pastor, Y. Ma, A. Kafizas, T. E. Rosser, M. T. Mayer, E. Reisner, M. Grätzel, V. S. Batista, J. R. Durrant, Nat. Chem. (2019). doi: 10.1038/s41557-019-0347-1
61. Y. Hermans, A. Klein, K. Ellmer, R. van de Krol, T. Toupance, W. Jaegermann, J. Phys. Chem. C **122** (2018) 20861.
62. M. Borgwardt, S. T. Omelchenko, M. Favaro, P. Plate, C. Höhn, D. Abou-Ras, K. Schwarzburg, R. van de Krol, H. A. Atwater, N. S. Lewis, R. Eichberger, D. Friedrich, Nat. Commun. **10** (2019) 2106.
63. W.-H. Cheng, M. H. Richter, M. M. May, J. Ohlmann, D. Lackner, F. Dimroth, T. Hannappel, H. A. Atwater, H.-J. Lewerenz, ACS Energy Lett. **3** (2018) 1795.
64. M. M. May, H.-J. Lewerenz, D. Lackner, F. Dimroth, T. Hannappel, Nat. Commun. **6** (2015) 8286.
65. W. Mönch, Electronic Properties of Semiconductor Interfaces, Springer-Verlag, Heidelberg (2003).
66. C. A. Sebenne, In: Photoemission of Semiconductor Surfaces in Optical Properties of Semiconductors, M. Balkanski (Ed.). North-Holland, Amsterdam (1994).
67. E. H. Rhoderick, R. H. Williams, Metal-Semiconductor Contacts, Clarendon Press, Oxford (1988).
68. B. L. Sharma (Ed.): Metal Semiconductor Schottky Barrier Junctions and their Applications, Plenum Press, New York (1984).
69. S. M. Sze, Physics of Semiconductor Devices, John Wiley & Sons, New York (1981).
70. L. J. Brillson, Surf. Sci. Rep. **2** (1982) 123.
71. H. Lüth, Surfaces and Interfaces of Solids, Springer-Verlag, Berlin (1993).
72. M. L. Rosenbluth, N. S. Lewis, J. Phys. Chem. **93** (1989) 3735.
73. R. Hunger, T. Schulmeyer, A. Klein, W. Jaegermann, M. Lebedev, K. Sakurai, S. Niki, Thin Solid Films **480-481** (2005) 218.
74. J. Guo, W. Jaegermann, J. Electron Spectrosc. **221** (2017) 1.
75. F. Lin, S. W. Boettcher, Nat. Mater. **13** (2014) 81.
76. A. M. Cowley, S. M. Sze, J. Appl. Phys. **36** (1965) 3212.
77. A. J. Appleby, A. E. Delahoy, S. C. Gau, O. J. Murphy, M. Kapur, J. O. M. Bockris, Energy **10** (1985) 871.
78. A. E. Delahoy, S. C. Gau, O. J. Murphy, M. Kapur, J. O. M. Bockris, Int. J. Hydrogen Energ. **10** (1985) 113.
79. G. H. Lin, M. Kapur, R. C. Kainthla, J. O. M. Bockris, Appl. Phys. Lett. **55** (1989) 386.
80. R. E. Rocheleau, E. L. Miller, A. Misra, Energ. Fuel **12** (1998) 3.
81. O. Khaselev, A. Bansal, J. A. Turner, Int. J. Hydrogen Energ. **26** (2001) 127.
82. E. L. Miller, R. E. Rocheleau, X. M. Deng, Int. J. Hydrogen Energ. **28** (2003) 615.
83. Y. Yamada, N. Matsuki, T. Ohmori, H. Mametsuka, M. Kondo, A. Matsuda, E. Suzuki, Int. J. Hydrogen Energ. **28** (2003) 1167.
84. N. A. Kelly, T. L. Gibson, Int. J. Hydrogen Energ. **31** (2006) 1658.
85. M. G. Walter, E. L. Warren, J. R. McKone, S. W. Boettcher, Q. X. Mi, E. A. Santori, N. S. Lewis, Chem. Rev. **110** (2010) 6446.

86. F. Finger, K. Welter, F. Urbain, V. Smirnov, B. Kaiser, W. Jaegermann, Z. Phys. Chem. (Received April 26, 2019; accepted July 26, 2019). doi: 10.1515/zpch-2019-1453
87. F. Urbain, V. Smirnov, J.-P. Becker, A. Lambertz, U. Rau, F. Finger, Sol. Energy Mat. Sol. Cells **145** (2016) 142.
88. F. Urbain, V. Smirnov, J.-P. Becker, A. Lambertz, F. Yang, J. Ziegler, B. Kaiser, W. Jaegermann, U. Rau, F. Finger, Energy Environ. Sci. **9** (2016) 145.
89. F. Urbain, V. Smirnov, J.-P. Becker, U. Rau, F. Finger, J. Ziegler, B. Kaiser, W. Jaegermann, J. Mat. Res. **29** (2014) 2605.
90. M. A. Green, K. Emery, Y. Hishikawa, W. Warta, E. D. Dunlop, Prog. Photovoltaics Res. Appl. **23** (2015) 1.
91. A. Lambertz, V. Smirnov, T. Merdzhanova, K. Ding, S. Haas, G. Jost, R. E. I. Schropp, F. Finger, U. Rau, Sol. Energy Mater. Sol. Cells **119** (2013) 134.
92. V. Smirnov, A. Lambertz, S. Tillmanns, F. Finger, Canadian J. Phys. **92** (2014) 932.
93. J. Ziegler, B. Kaiser, W. Jaegermann, F. Urbain, J.-P. Becker, V. Smirnov, F. Finger, ChemPhysChem **15** (2014) 4026.
94. M. J. Muñoz-Portero, J. García-Antón, J. L. Guiñón, R. Leiva-García, Corros. Sci. **53** (2011) 1440.
95. L. Forro, O. Chauvet, D. Emin, L. Zuppiroli, H. Berger, F. Lévy, J. Appl. Phys. **75** (1994) 633.
96. J. Ziegler, Photoelektrosynthese von Wasserstoff mit Silizium-Dünnschicht-Tandemsolarzellen, Doctoral Thesis, Technische Universität Darmstadt (2015).
97. J. M. Hill, D. G. Royce, C. S. Fadley, L. F. Wagner, F. J. Grunthaner, Chem. Phys. Lett. **44** (1976) 225.
98. A. Klein, T. Mayer, A. Thissen, W. Jaegermann, Bunsenmagazin **10** (2008) 124.
99. A. Klein, F. Säuberlich, Surfaces and Interfaces of Sputter-Deposited ZnO Films in Transparent Conductive Zinc Oxide: Basics and Applications in Thin Film Solar Cells, K. Ellmer, A. Klein and B. Rech (Eds.). Springer-Verlag, Berlin (2008), P. 125.
100. J. Klett, J. Ziegler, A. Radetinac, B. Kaiser, R. Schaefer, W. Jaegermann, F. Urbain, J.-P. Becker, V. Smirnov, F. Finger, Phys. Chem. Chem. Phys. **18** (2016) 10751.
101. C. C. Fulton, G. Lucovsky, R. J. Nemanich, J. Vac. Sci. Technol. **20** (2002) 1726.
102. D. A. Muller, T. Sorsch, S. Moccio, F. H. Baumann, K. Evans-Lutterodt, G. Timp, Nature **399** (1999) 758.
103. J. Ziegler, F. Yang, S. Wagner, B. Kaiser, W. Jaegermann, F. Urbain, J.-P. Becker, V. Smirnov, F. Finger, Appl. Surf. Sci. **389** (2016) 73.
104. B. Seger, T. Pedersen, A. B. Laursen, P. C. K. Vesborg, O. Hansen, I. Chorkendorff, J. Am. Chem. Soc. **135** (2013) 1057.
105. B. Seger, D. S. Tilley, T. Pedersen, P. C. K. Vesborg, O. Hansen, M. Grätzel, I. Chorkendorff, RSC Adv. **3** (2013) 25902.
106. J. Klett, A. Eva, F. Heinz, B. Kaiser, W. Jaegermann, R. Schäfer, ChemCatChem **8** (2016) 345.
107. A. Eva, Metalorganic Chemical vapor Deposition of Platinum Nanoparticles for Water Electrolysis, Master of Science Thesis, Technische Universität Darmstadt (2014).
108. S. Trasatti, O. A. Petrii, J. Electroanal. Chem. **327** (1992) 353.
109. F. J. Vidal-Iglesias, R. M. Arán-Ais, J. Solla-Gullón, E. Herrero, J. M. Feliu, ACS Catal. **2** (2012) 901.
110. J. Klett, Interface and Catalyst Investigation for Solar Water Splitting, Doctoral thesis, Technische Universität Darmstadt (2016).

111. N. M. Markovia, S. T. Sarraf, H. A. Gasteiger, P. N. Ross, J. Chem. Soc. Faraday Trans. **92** (1996) 3719.
112. H. N. Nong, H. P. Tran, C. Spöri, M. Klingenhof, L. Frevel, T. Jones, T. Cottre, B. Kaiser, W. Jaegermann, R. Schlögl, D. Teschner, P. Strasser, Z. Phys. Chem. (accepted 2019).
113. T. Cottre, K. Welter, E. Ronge, V. Smirnov, F. Finger, C. Jooss, B. Kaiser, W. Jaegermann, Z. Phys. Chem. (accepted 2019).
114. E. Ronge, T. Cottre, K. Welter, V. Smirnov, N. Ottinger, F. Finger, B. Kaiser, W. Jaegermann, C. Jooss, Z. Phys. Chem. (accepted 2019).
115. F. Neuberger, J. Baranyai, T. Schmidt, T. Cottre, B. Kaiser, W. Jaegermann, R. Schäfer, Z. Phys. Chem. (accepted 2019).
116. F. Urbain, V. Smirnov, J. P. Becker, U. Rau, J. Ziegler, F. Yang, B. Kaiser, W. Jaegermann, S. Hoch, M. Blug, F. Finger, Chem. Phys. Lett. **638** (2015) 25.
117. M. A. Green, Third Generation Photovoltaics, Springer, Berlin (2003).